

Numerical solution of two dimensional scalar conservation laws using compact implicit numerical schemes *

Dagmar ŽÁKOVÁ¹ and Peter FROLKOVIČ²

¹Department of Mathematics and Descriptive Geometry, Slovak University of Technology in Bratislava (dagmar.zakova@stuba.sk)

²Department of Mathematics and Descriptive Geometry, Slovak University of Technology in Bratislava (peter.frolkovic@stuba.sk)

Abstract: This paper deals with the numerical solution of conservation laws in the two dimensional case using a novel compact implicit time discretization that enable applications of fast algebraic solvers. We present details for the second order accurate parametric scheme based on the finite volume method including simple variants of ENO (Essentially Non-Oscillatory) and WENO (Weighted Essentially Non-Oscillatory) approximations. We present numerical experiments for representative linear and nonlinear problems.

Key words: conservation law, second order accuracy, compact implicit scheme, advection equation, Burgers equation

1 Introduction

Time dependent partial differential equations are typically solved by numerical methods where the time discretization is applied separately from the spatial discretization. Such an approach has the advantage that well developed and implemented integration methods for numerical solution of ordinary differential equations (ODEs) can be used after the equation is discretized in space. Already at the level of ODEs, it is recognized that the explicit type of time discretization methods are not suitable for systems of ODEs of which the solution describes processes with different time scales. In such a case, the restriction on the size of the time step is no longer applicable if the fast processes require too small time steps only due to the stability constraints and not due to the accuracy requirements. A similar situation can occur when the time dependent solution in numerical simulations is approaching a stationary state, especially if some asymptotic preserving properties are expected from the numerical solution.

In the above mentioned cases, the well-known remedy is to apply implicit methods for the numerical solution of the ODEs that replace some explicit formulas to determine the numerical solution by discrete algebraic equations to be solved. This type of method is available with enhanced stability properties and offers, in an ideal case, the usage with the time steps having a size that is limited only by the accuracy requirements. The price to pay for such stability enhancement is strongly dependent on the efficiency with which the resulting discrete systems of algebraic equations can be solved.

Numerical methods based on the separate discretization of time and space have been well developed for hyperbolic systems. Concerning implicit methods (or their combinations with explicit methods), we can mention the class of Runge-Kutta (RK) methods used for hyperbolic problems in [18, 3, 4, 2, 1, 19, 17]. Furthermore, it is recognized that several improvements can be achieved if, opposite to standard RK methods, not only the values of the right hand side function are used, but also its derivatives. This approach is realized in the development of two- or multi-derivative RK methods [22] available also in the form of implicit methods [26, 12].

The approach of multi-derivative RK methods is shared with other type of time discretization methods that exploit finite Taylor series expansions of the solution with the so-called Lax-Wendroff (or Cauchy-Kowalevskaya) procedure when the time derivatives are replaced by corresponding derivatives of the right hand side function. The methods based on the LW procedure offer a great opportunity to couple the time and space discretizations by approximating each term in the Taylor series by different space discretizations [20, 22, 24, 15, 26]. This

*The work was supported by the grant VEGA 1/0314/23 and APVV-19-0460.

coupling is significantly exploited in methods that use mixed spatial-temporal derivatives in the Lax-Wendroff procedure to obtain schemes with a more compact stencil [28, 5, 6].

As shown in [9, 11, 10], the idea of implicit time discretization using the LW procedure involving the mixed spatial-temporal derivatives can be used not only to enhance the stability of the method but also to improve the solvability of the resulting algebraic systems. In particular, a compact high-resolution finite difference method for hyperbolic problems in the one-dimensional case is presented in [10] in connection with the fractional step method [16] where the Jacobian matrix has a convenient structure, and therefore efficient solvers like the fast sweeping method [16] can be used. In this work we extend the approach of [10] to two-dimensional finite volume methods. Opposite to [16, 10], we do not use the fractional-time step method that can decrease the accuracy due to time splitting errors [14]. To further increase the efficiency of the method, we apply the predictor-corrector approach to compute the parameters in the ENO and WENO schemes as used in [19].

The paper is organized as follows. In Section 2 we introduce the scalar conservation laws for two dimensional case and a general form of the finite volume method for its numerical solution. In Section 3 we derive a parametric form of a second order accurate scheme. In Section 4 we extend the schemes to the framework of High resolution scheme with the use of the ENO (Essentially Non-Oscillatory) and WENO (Weighted Essentially Non-Oscillatory) approximations. Finally, in Section 5 we illustrate the properties of the presented schemes with several numerical experiments.

2 Mathematical model and finite volume method

First, we consider the scalar nonlinear hyperbolic equation in the form

$$\partial_t u + \nabla \cdot \mathbf{f}(u) = 0, \quad (1)$$

with $\mathbf{f}(u) = (f(u), g(u))$ being the vector flux function, so (1) can be written in the form

$$\partial_t u + \partial_x f(u) + \partial_y g(u) = 0. \quad (2)$$

with $u = u(x, y, t)$ being the unknown function for $t \in (0, T)$, and $x \in (x_L, x_R) \subset \mathbb{R}$, $y \in (y_L, y_R) \subset \mathbb{R}$. The initial condition is prescribed by $u(x, y, 0) = u^0(x, y)$ and the boundary conditions are defined at the inflow boundaries as

$$u(x_L, y, t) = u_{x_L}(y, t), \quad u(x, y_L, t) = u_{y_L}(x, t), \quad u(x_R, y, t) = u_{x_R}(y, t), \quad u(x, y_R, t) = u_{y_R}(x, t). \quad (3)$$

Next, we introduce a numerical discretization to solve the equation (2). The discretization is done in space and time using the following notation. We denote $t^n = n\tau$, $n = 0, 1, \dots, N$ for a chosen N and $\tau > 0$ with $t^{n+1/2} = t^n + \tau/2$. The spatial discretization is based on the finite volume method [14]. For simplicity, we assume the computational domain defined for $x, y \in (x_L, x_R)$ that is divided into finite volumes of the form $I_{i,j} = (x_{i-1/2}, x_{i+1/2}) \times (y_{j-1/2}, y_{j+1/2})$ with the regular square grid, where $x_{i-1/2} = x_L + ih - h/2$ and $y_{j-1/2} = y_L + jh - h/2$ with $i, j = 1, 2, \dots, M$ for the chosen M and $h = (x_R - x_L)/M$.

The main idea behind the finite volume method is to integrate the differential equation (2) over $I_{i,j} \times (t^n, t^{n+1})$

$$\int_{t^n}^{t^{n+1}} \int_{I_{i,j}} (\partial_t u + \partial_x f(u) + \partial_y g(u)) dx dy dt = 0. \quad (4)$$

Using the divergence theorem in (4) with $\mathbf{n}(s) = (n^x(s), n^y(s))$ be the outward-pointing unit normal vector to the boundary $\partial I_{i,j}$ of the finite volume $I_{i,j}$ at a point $(x(s), y(s))$, we obtain

$$\begin{aligned} \int_{I_{i,j}} (\partial_x f(u) + \partial_y g(u)) dx dy &= \int_{\partial I_{i,j}} (n^x(s)f(u) + n^y(s)g(u)) ds \\ &= \int_{y_{j-1/2}}^{y_{j+1/2}} f(u(x_{i+1/2}, y, t)) dy - \int_{y_{j-1/2}}^{y_{j+1/2}} f(u(x_{i-1/2}, y, t)) dy \\ &\quad + \int_{x_{i-1/2}}^{x_{i+1/2}} g(u(x, y_{j+1/2}, t)) dx - \int_{x_{i-1/2}}^{x_{i+1/2}} g(u(x, y_{j-1/2}, t)) dx. \end{aligned} \quad (5)$$

Next, using the notation for the space and time averaged values defined as

$$\begin{aligned}\tilde{u}_{i,j}^n &:= \frac{1}{h^2} \int_{I_{i,j}} u(x, y, t^n) dx dy, \\ f_{i+1/2,j} &:= \frac{1}{\tau h} \int_{t^n}^{t^{n+1}} \int_{y_{j-1/2}}^{y_{j+1/2}} f(u(x_{i+1/2}, y, t)) dy dt, \\ g_{i,j+1/2} &:= \frac{1}{\tau h} \int_{t^n}^{t^{n+1}} \int_{x_{i-1/2}}^{x_{i+1/2}} g(u(x, y_{j+1/2}, t)) dx dt,\end{aligned}\tag{6}$$

one can rewrite (4) to the equivalent form,

$$\tilde{u}_{i,j}^{n+1} - \tilde{u}_{i,j}^n + \frac{\tau}{h}(f_{i+1/2,j} - f_{i-1/2,j}) + \frac{\tau}{h}(g_{i,j+1/2} - g_{i,j-1/2}) = 0.\tag{7}$$

To obtain a numerical scheme, one has to approximate the averaged fluxes $f_{i+1/2,j}$ and $g_{i,j+1/2}$ in (7) using some numerical fluxes $F_{i+1/2,j} \approx f_{i+1/2,j}$, $G_{i,j+1/2} \approx g_{i,j+1/2}$. As we aim to obtain the second order accuracy, we consider midpoint quadrature rules to approximate the integrals in (6). Using $u_{i,j}^n \approx \tilde{u}_{i,j}^n$, the numerical scheme takes then the form

$$u_{i,j}^{n+1} - u_{i,j}^n + \frac{\tau}{h}(F_{i+1/2,j} - F_{i-1/2,j}) + \frac{\tau}{h}(G_{i,j+1/2} - G_{i,j-1/2}) = 0.\tag{8}$$

There are several ways how to construct the numerical flux, and, for our purposes, we choose the Godunov flux [23, 14], where the flux $F_{i+1/2,j}$ is represented at time $t^{n+1/2}$ as

$$F_{i+1/2,j} = H(u_{i+1/2,j}^{n+1/2,-}, u_{i+1/2,j}^{n+1/2,+}),\tag{9}$$

and the flux $G_{i,j+1/2}$ similarly as

$$G_{i,j+1/2} = H(u_{i,j+1/2}^{n+1/2,-}, u_{i,j+1/2}^{n+1/2,+}),\tag{10}$$

with the numerical flux function H defined by

$$H(u^-, u^+) = \begin{cases} \min_{u^- \leq u \leq u^+} h(u) & \text{if } u^- \leq u^+ \\ \max_{u^+ \leq u \leq u^-} h(u) & \text{if } u^- > u^+ \end{cases}\tag{11}$$

where $h = f$ for (9) and $h = g$ for (10). Finally, one has to propose one-sided numerical approximations

$$u_{i+1/2,j}^{n+1/2,\pm} \approx \lim_{x \rightarrow x_{i+1/2}^\pm} u(x, y_j, t^{n+1/2}), \quad u_{i,j+1/2}^{n+1/2,\pm} \approx \lim_{y \rightarrow y_{j+1/2}^\pm} u(x_i, y, t^{n+1/2}),$$

that we aim to define using the values of numerical solution at time levels t^n and t^{n+1} using upwind based approximations similarly to [7, 10].

We also define such approximations for the numerical solutions of the two dimensional linear advection equation [25], where \mathbf{f} from (1) is formally represented by $\mathbf{f} = \vec{v}u$,

$$\partial_t u + \nabla \cdot (\vec{v}u) = 0.\tag{12}$$

We consider a space dependent given velocity field $\vec{v} = \vec{v}(x, y) = (v(x, y), w(x, y))$, so the flux function \mathbf{f} in (1) also depends on the space variables that we consider only for the linear advection. The problem takes the form

$$\partial_t u + \partial_x(vu) + \partial_y(wu) = 0.\tag{13}$$

To define numerical flux function for (13) we denote

$$v_{i\pm 1/2,j} := v(x_{i\pm 1/2}, y_j), \quad w_{i,j\pm 1/2} := w(x_i, y_{j\pm 1/2}).\tag{14}$$

Furthermore, we will apply the splitting of the velocity vector field, which is performed as

$$\begin{aligned}v &= v^+ + v^-, & \text{with } v^+ &:= \max(0, v), \quad v^- := \min(0, v), \\ w &= w^+ + w^-, & \text{with } w^+ &:= \max(0, w), \quad w^- := \min(0, w),\end{aligned}\tag{15}$$

and the numerical fluxes (8) will be defined compatibly with (11) as

$$\begin{aligned} F_{i+1/2,j} &= v_{i+1/2,j}^+ u_{i+1/2,j}^{n+1/2,-} + v_{i+1/2,j}^- u_{i+1/2,j}^{n+1/2,+}, \\ G_{i,j+1/2} &= w_{i,j+1/2}^+ u_{i,j+1/2}^{n+1/2,-} + w_{i,j+1/2}^- u_{i,j+1/2}^{n+1/2,+}, \end{aligned} \quad (16)$$

and the numerical scheme (8) will transform into the form

$$\begin{aligned} u_{i,j}^{n+1} - u_{i,j}^n &+ \frac{\tau}{h} (v_{i+1/2,j}^+ u_{i+1/2,j}^{n+1/2,-} - v_{i-1/2,j}^+ u_{i-1/2,j}^{n+1/2,-}) + \frac{\tau}{h} (w_{i,j+1/2}^+ u_{i,j+1/2}^{n+1/2,-} - w_{i,j-1/2}^+ u_{i,j-1/2}^{n+1/2,-}) \\ &+ \frac{\tau}{h} (v_{i+1/2,j}^- u_{i+1/2,j}^{n+1/2,+} - v_{i-1/2,j}^- u_{i-1/2,j}^{n+1/2,+}) + \frac{\tau}{h} (w_{i,j+1/2}^- u_{i,j+1/2}^{n+1/2,+} - w_{i,j-1/2}^- u_{i,j-1/2}^{n+1/2,+}) = 0. \end{aligned} \quad (17)$$

Note that the simplest first order accurate numerical scheme uses the approximations

$$\begin{aligned} u_{i+1/2,j}^{n+1/2,-} &= u_{i,j}^{n+1}, & u_{i+1/2,j}^{n+1/2,+} &= u_{i+1,j}^{n+1}, \\ u_{i,j+1/2}^{n+1/2,-} &= u_{i,j}^{n+1}, & u_{i,j+1/2}^{n+1/2,+} &= u_{i,j+1}^{n+1}. \end{aligned} \quad (18)$$

3 The second order accurate parametric compact implicit scheme

In this section, we present the parametric form of the second order accurate scheme in time and space that can be later used in the framework of high resolution schemes. As discussed above, one has to define the approximations $u_{i+1/2,j}^{n+1/2,\pm}$ and $u_{i,j+1/2}^{n+1/2,\pm}$ based on the upwind approach. For simplicity of the derivation, we will treat in detail only the derivation for the values $u_{i+1/2,j}^{n+1/2,-}$ and $u_{i,j+1/2}^{n+1/2,-}$. Similarly, one can handle the values $u_{i+1/2,j}^{n+1/2,+}$ and $u_{i,j+1/2}^{n+1/2,+}$ for which we will present only the final definitions.

To approximate the values $u_{i+1/2,j}^{n+1/2,-}$ and $u_{i,j+1/2}^{n+1/2,-}$ up to the second order of accuracy, we apply finite Taylor series [7]

$$u(x_{i+1/2}, y_j, t^{n+1/2}) = u(x_i, y_j, t^{n+1}) + \frac{h}{2} \partial_x u(x_i, y_j, t^{n+1}) - \frac{\tau}{2} \partial_t u(x_i, y_j, t^{n+1}) + \mathcal{O}(h^2, \tau^2) \quad (19)$$

and

$$u(x_i, y_{j+1/2}, t^{n+1/2}) = u(x_i, y_j, t^{n+1}) + \frac{h}{2} \partial_y u(x_i, y_j, t^{n+1}) - \frac{\tau}{2} \partial_t u(x_i, y_j, t^{n+1}) + \mathcal{O}(h^2, \tau^2). \quad (20)$$

Similarly to [7], we do not replace the time derivative using the Lax-Wendroff procedure, but we approximate (19) and (20) directly. Formally, the desired numerical values would then be defined as

$$\begin{aligned} u_{i+1/2,j}^{n+1/2,-} &= u_{i,j}^{n+1} + \frac{h}{2} \partial_x u_{i,j}^{n+1} - \frac{\tau}{2} \partial_t u_{i,j}^{n+1}, \\ u_{i,j+1/2}^{n+1/2,-} &= u_{i,j}^{n+1} + \frac{h}{2} \partial_y u_{i,j}^{n+1} - \frac{\tau}{2} \partial_t u_{i,j}^{n+1}, \end{aligned} \quad (21)$$

where we express the approximations $\partial_x u_{i,j}^{n+1}$, $\partial_y u_{i,j}^{n+1}$ and $\partial_t u_{i,j}^{n+1}$ as a linear combination of different approximation choices [10] using parameters $\omega \in [0, 1]$, namely,

$$\begin{aligned} u_{i+1/2,j}^{n+1/2,-} &= u_{i,j}^{n+1} + \frac{1}{2} (\omega^{x,-} (u_{i,j}^{n+1} - u_{i-1,j}^{n+1}) + (1 - \omega^{x,-}) (u_{i+1,j}^{n+1} - u_{i,j}^{n+1})) \\ &\quad - \frac{1}{2} (\omega^{x,-} (u_{i,j}^{n+1} - u_{i,j}^n) + (1 - \omega^{x,-}) (u_{i+1,j}^{n+1} - u_{i+1,j}^n)) \\ &= u_{i,j}^{n+1} - \frac{1}{2} (\omega^{x,-} (u_{i-1,j}^{n+1} - u_{i,j}^n) + (1 - \omega^{x,-}) (u_{i,j}^{n+1} - u_{i+1,j}^n)), \end{aligned} \quad (22)$$

$$\begin{aligned} u_{i,j+1/2}^{n+1/2,-} &= u_{i,j}^{n+1} + \frac{1}{2} (\omega^{y,-} (u_{i,j}^{n+1} - u_{i,j-1}^{n+1}) + (1 - \omega^{y,-}) (u_{i,j+1}^{n+1} - u_{i,j}^{n+1})) \\ &\quad - \frac{1}{2} (\omega^{y,-} (u_{i,j}^{n+1} - u_{i,j}^n) + (1 - \omega^{y,-}) (u_{i,j+1}^{n+1} - u_{i,j+1}^n)) \\ &= u_{i,j}^{n+1} - \frac{1}{2} (\omega^{y,-} (u_{i,j-1}^{n+1} - u_{i,j}^n) + (1 - \omega^{y,-}) (u_{i,j}^{n+1} - u_{i,j+1}^n)). \end{aligned} \quad (23)$$

Notice that we have managed to obtain a compact stencil as the values $u_{i+1,j}^{n+1}$ and $u_{i,j+1}^{n+1}$ in (22) and (23) are canceled. This is also the substantial difference to the approach given in [7]. Two particular choices of parameters $\omega^{x,-} \in [0, 1]$ and $\omega^{y,-} \in [0, 1]$ do not use the full stencil of the approximations in (22) and (23) that we use later conveniently for ENO approximation [23]. In particular, with the value $\omega^{x,-} = 0$ and $\omega^{y,-} = 0$ we create a "central" kind of discretization and for $\omega^{x,-} = 1$ (and $\omega^{y,-} = 1$) the "upwind" one.

Very similarly, one obtains the numerical approximations of $u_{i+1/2,j}^{n+1/2,+}$ and $u_{i,j+1/2}^{n+1/2,+}$ as

$$\begin{aligned} u_{i+1/2,j}^{n+1/2,+} &= u_{i+1,j}^{n+1} - \frac{1}{2}(\omega^{x,+}(u_{i+2,j}^{n+1} - u_{i+1,j}^n) + (1 - \omega^{x,+})(u_{i+1,j}^{n+1} - u_{i,j}^n)), \\ u_{i,j+1/2}^{n+1/2,+} &= u_{i,j+1}^{n+1} - \frac{1}{2}(\omega^{y,+}(u_{i,j+2}^{n+1} - u_{i,j+1}^n) + (1 - \omega^{y,+})(u_{i,j+1}^{n+1} - u_{i,j}^n)). \end{aligned} \quad (24)$$

We collect all parameters by $\boldsymbol{\omega} = (\omega^{x,-}, \omega^{x,+}, \omega^{y,-}, \omega^{y,+})$.

Now, to finalize the second order accurate compact implicit scheme, we express the numerical fluxes in (8) using (9) and (10) with the numerical approximations $u_{i+1/2,j}^{n+1/2,\pm}$, $u_{i,j+1/2}^{n+1/2,\pm}$ from (22), (23), and (24).

The discretization scheme creates a system of algebraic equations that can be solved iteratively using the fast sweeping method, where each sweeping iteration is given by one Gauss-Seidel iteration applied sequentially with alternating index directions across the computational domain [27, 16]. In particular, we use four different "sweeps" from each corner of a rectangular domain:

$$\begin{aligned} i &= 1, \dots, M, \quad j = 1, \dots, M \\ i &= M, \dots, 1, \quad j = 1, \dots, M \\ i &= M, \dots, 1, \quad j = M, \dots, 1 \\ i &= 1, \dots, M, \quad j = M, \dots, 1 \end{aligned} \quad (25)$$

where each *sweep* represents the (linear or nonlinear) Gauss-Seidel method (GS) with the given ordering. Note that in the case of a nonlinear flux function \mathbf{f} , one has to solve a nonlinear algebraic equation for each pair of indices i and j in the sweeps. When solving the linear advection equation (13) with a constant velocity, the solution of the system of algebraic equations can be obtained by performing only one particular sweep in (25). In general, to reduce the absolute error of the iterative fast sweeping method, more than four sweeping Gauss-Seidel iterations (4GS) shall be used for each time step.

4 High resolution schemes

For discontinuous initial conditions, or when shocks are present in the solution of (2), unphysical oscillations may occur in numerical solutions if the numerical methods from the previous section are used, as illustrated in Figure 1. To avoid such oscillations, we use the parametric form of the second order scheme to choose the values of the parameters $\boldsymbol{\omega}$ in each numerical flux differently. i.e., depending on the numerical solution [23, 10].

Let $\omega^{x,\pm} = \omega_{i,j}^{x,\pm} \in [0, 1]$ and $\omega^{y,\pm} = \omega_{i,j}^{y,\pm} \in [0, 1]$ for each $I_{i,j}$ in (22) and (23), be the free parameters that we aim to determine. Moreover, as is known from the literature [7, 19, 10], the unphysical oscillations occur not only due to an inappropriate fixed choice of space reconstruction, but also because of the fixed time reconstruction, therefore, similarly to [10], we add another numerical parameter $\mathbf{l} = (l^{x,\pm}, l^{y,\pm})$, which, if necessary, can limit the second order space reconstruction to the first order form of the scheme that produces numerical solutions free of unphysical oscillations, and, again, it is defined at each $I_{i,j}$ in a form $l_{i,j}^{x,\pm}, l_{i,j}^{y,\pm} \in [0, 1]$. Notice that the values $\boldsymbol{\omega}$ and \mathbf{l} also change at each time step, which we do not emphasize in the notation.

In summary, the approximation (22) and (23) will transform into the form

$$\begin{aligned} u_{i+1/2,j}^{n+1/2,-} &= u_{i,j}^{n+1} - \frac{l_{i,j}^{x,-}}{2}(\omega_{i,j}^{x,-}(u_{i-1,j}^{n+1} - u_{i,j}^n) + (1 - \omega_{i,j}^{x,-})(u_{i,j}^{n+1} - u_{i+1,j}^n)), \\ u_{i,j+1/2}^{n+1/2,-} &= u_{i,j}^{n+1} - \frac{l_{i,j}^{y,-}}{2}(\omega_{i,j}^{y,-}(u_{i,j-1}^{n+1} - u_{i,j}^n) + (1 - \omega_{i,j}^{y,-})(u_{i,j}^{n+1} - u_{i,j+1}^n)), \end{aligned} \quad (26)$$

and for (24)

$$\begin{aligned} u_{i+1/2,j}^{n+1/2,+} &= u_{i+1,j}^{n+1} - \frac{l_{i+1,j}^{x,+}}{2}(\omega_{i+1,j}^{x,+}(u_{i+2,j}^{n+1} - u_{i+1,j}^n) + (1 - \omega_{i+1,j}^{x,+})(u_{i+1,j}^{n+1} - u_{i,j}^n)), \\ u_{i,j+1/2}^{n+1/2,+} &= u_{i,j+1}^{n+1} - \frac{l_{i,j+1}^{y,+}}{2}(\omega_{i,j+1}^{y,+}(u_{i,j+2}^{n+1} - u_{i,j+1}^n) + (1 - \omega_{i,j+1}^{y,+})(u_{i,j+1}^{n+1} - u_{i,j}^n)). \end{aligned} \quad (27)$$

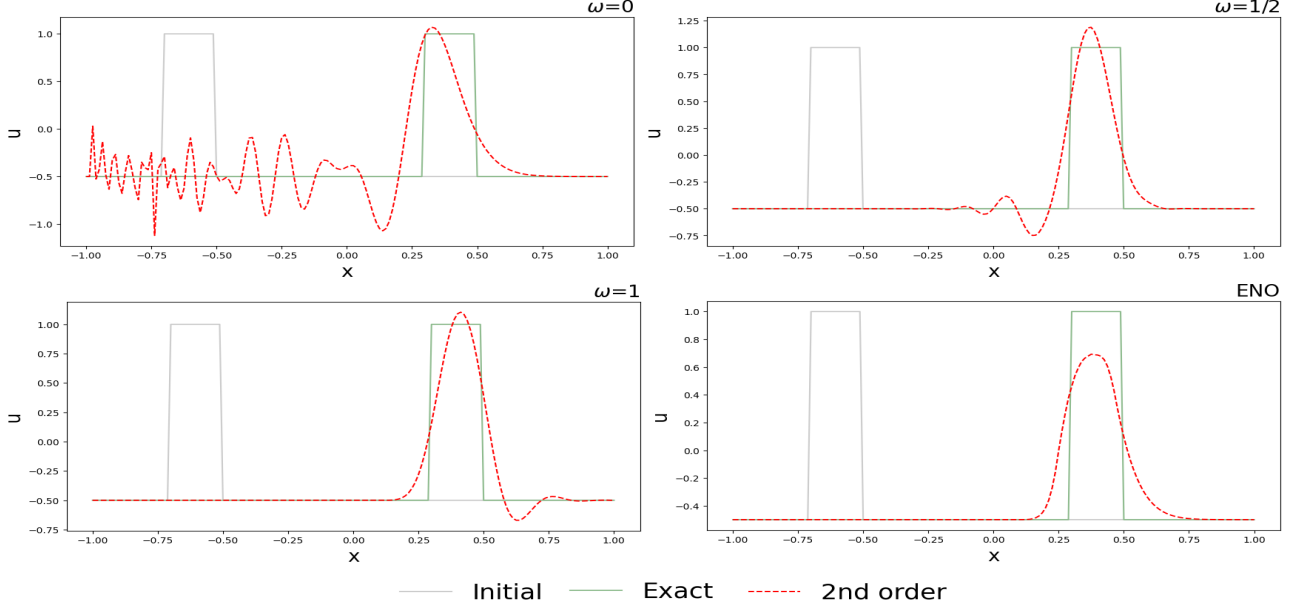


Figure 1: Cross-sectional views of a numerical solutions of a linear advection equation, with the discontinuous initial condition, obtained using the second order accurate scheme and the fixed choices of $\omega^{x,\pm}, \omega^{y,\pm} = 0, 1/2, 1$, sequentially, at each $I_{i,j}$, and using the ENO scheme. The Courant number equals 5. For the description of the example see the section 5 on numerical experiments.

The high-resolution scheme is then defined by (8) - (11) with the interface values given in (26) - (27).

Concerning the space reconstruction, we present in the next sections two standard choices - the Essentially Non-Oscillatory (ENO) method and the Weighted ENO (WENO) method. The value of ω for the ENO method will depend on the following ratios in $\mathbf{r} = (r_{i,j}^{x,\pm}, r_{i,j}^{y,\pm})$,

$$\begin{aligned}
 r_{i,j}^{x,-} &= \frac{u_{i-1,j}^{n+1} - u_{i,j}^n}{u_{i,j}^{n+1} - u_{i+1,j}^n}, & r_{i,j}^{x,+} &= \frac{u_{i+1,j}^{n+1} - u_{i,j}^n}{u_{i,j}^{n+1} - u_{i-1,j}^n}, \\
 r_{i,j}^{y,-} &= \frac{u_{i,j-1}^{n+1} - u_{i,j}^n}{u_{i,j}^{n+1} - u_{i,j+1}^n}, & r_{i,j}^{y,+} &= \frac{u_{i,j+1}^{n+1} - u_{i,j}^n}{u_{i,j}^{n+1} - u_{i,j-1}^n},
 \end{aligned} \tag{28}$$

the WENO method will depend on nominators and denominators in the ratios in \mathbf{r} .

Once the solution dependent values of ω are computed, they are used together with the ratios in (28) for the definition of the parameters $l_{i,j}^{x,-}, l_{i,j}^{y,-}$ [10] that are determined by

$$\begin{aligned}
 l_{i,j}^{x,-} &= \min \left\{ 1, \max \left\{ 0, \left(\omega_{i,j}^{x,-} + \frac{1 - \omega_{i,j}^{x,-}}{r_{i,j}^{x,-}} \right)^{-1} \left(\frac{2}{C} + l_{i-1,j}^{x,-} (\omega_{i-1,j}^{x,-} r_{i-1,j}^{x,-} + 1 - \omega_{i-1,j}^{x,-}) \right) \right\} \right\}, \\
 l_{i,j}^{y,-} &= \min \left\{ 1, \max \left\{ 0, \left(\omega_{i,j}^{y,-} + \frac{1 - \omega_{i,j}^{y,-}}{r_{i,j}^{y,-}} \right)^{-1} \left(\frac{2}{C} + l_{i,j-1}^{y,-} (\omega_{i,j-1}^{y,-} r_{i,j-1}^{y,-} + 1 - \omega_{i,j-1}^{y,-}) \right) \right\} \right\},
 \end{aligned} \tag{29}$$

and similarly for $l_{i,j}^{x,+}, l_{i,j}^{y,+}$, with the parameter C being the Courant like number which one can define differently for linear and nonlinear case. In our case, for the nonlinear Burgers equation (see later), the parameter C is defined by

$$C = \max \left\{ 1, \frac{\tau}{h} \max_u |f'(u)| + \frac{\tau}{h} \max_u |g'(u)| \right\}. \tag{30}$$

For the linear advection (13) with the velocity field $\vec{v} = (v(x, y), w(x, y))$, the parameter C is given as a sum of Courant like numbers at the outflow boundaries,

$$C = C_{i+1/2,j}^{x,+} - C_{i-1/2,j}^{x,-} + C_{i,j+1/2}^{y,+} - C_{i,j-1/2}^{y,-}, \tag{31}$$

using the velocities from (15),

$$\begin{aligned} C_{i+1/2,j}^{x,+} &= \frac{\tau}{h} v_{i+1/2,j}^+, & C_{i-1/2,j}^{x,-} &= \frac{\tau}{h} v_{i-1/2,j}^-, \\ C_{i,j+1/2}^{y,+} &= \frac{\tau}{h} w_{i,j+1/2}^+, & C_{i,j-1/2}^{y,-} &= \frac{\tau}{h} w_{i,j-1/2}^-. \end{aligned} \quad (32)$$

In Appendix, we derive conditions for the parameters ω and l under which the numerical scheme (17) with (26) and (27) for divergence free velocity fields, i.e., $\nabla \cdot \vec{v} = 0$, produces numerical solutions fulfilling discrete minimum and maximum principle. These conditions motivate our definitions of (29), see also [10] for the nonlinear case.

In the next subsections, we present the simplest ENO and WENO procedures from [23] adapted to our compact implicit form [10]. As the parameters $\omega_{i,j}^{x,\pm}, \omega_{i,j}^{y,\pm}$ will depend on the unknown value $u_{i,j}^{n+1}$ (28), we propose its computations using a predictor-corrector approach [19].

4.1 ENO procedure

With an appropriate choice of $\omega_{i,j}^{x,\pm}, \omega_{i,j}^{y,\pm}$ being either 0 or 1, we can define a so-called Essentially Non-Oscillatory (ENO) scheme [23]. The choice can be based on the ratios in \mathbf{r} (28),

$$\begin{aligned} \omega_{i,j}^{x,-} &= \begin{cases} 1 & \text{if } |r_{i,j}^{x,-}| \leq 1 \\ 0 & \text{otherwise} \end{cases}, & \omega_{i,j}^{x,+} &= \begin{cases} 1 & \text{if } |r_{i,j}^{x,+}| \leq 1 \\ 0 & \text{otherwise} \end{cases}, \\ \omega_{i,j}^{y,-} &= \begin{cases} 1 & \text{if } |r_{i,j}^{y,-}| \leq 1 \\ 0 & \text{otherwise} \end{cases}, & \omega_{i,j}^{y,+} &= \begin{cases} 1 & \text{if } |r_{i,j}^{y,+}| \leq 1 \\ 0 & \text{otherwise} \end{cases}. \end{aligned} \quad (33)$$

The corrector-predictor procedure to evaluate the ratios in \mathbf{r} dependent on $u_{i,j}^{n+1}$ is composed of the following steps:

1. Calculate a predicted value $u_{i,j}^{n+1}$, using the numerical scheme (8) - (11) and (22) - (24) with the fixed values $\omega^{x,\pm} = \omega^{y,\pm} = 0$. The calculation involves performing (at least) four sequential Gauss-Seidel (4GS) iterations (25).
2. The corrector step consists of (at least) 4GS iterations in prescribed order (25), where for each of the iterations, one needs to perform:
 - 2.1 Calculate $r_{i,j}^{x,\pm}$ and $r_{i,j}^{y,\pm}$ from (28) using the predicted value of $u_{i,j}^{n+1}$.
 - 2.2 Set $\omega_{i,j}^{x,\pm}$ and $\omega_{i,j}^{y,\pm}$ with (33) based on the calculated \mathbf{r} in the step 2.1; and, afterwards, calculate the values $l_{i,j}^{x,\pm}, l_{i,j}^{y,\pm}$ from (29).
 - 2.3 Calculate the corrected value $u_{i,j}^{n+1}$ using the obtained values $\omega_{i,j}^{x,\pm}, \omega_{i,j}^{y,\pm}$ and $l_{i,j}^{x,\pm}$ and $l_{i,j}^{y,\pm}$ in the step 2.2.
 - 2.4 Set either the corrected value as a new predictor and perform again Step 2, or accept the corrected values.

We compute several numerical experiments (see Section 5) with the ENO scheme for which we investigate, among others, the behavior of the fast sweeping method depending on the number of Gauss-Seidel iterations.

4.2 WENO procedure

To create a weighted essentially non-oscillatory scheme, we propose, again, a solution-dependent choice of $\omega_{i,j}^{x,\pm}, \omega_{i,j}^{y,\pm}$ as found in [20, 23] and adapted to compact implicit scheme. The WENO scheme is used to achieve a smoother choice, comparing to the ENO scheme, between the „upwind” and „central” differences in (22) - (23) and (24), so $\omega_{i,j}^{x,\pm}, \omega_{i,j}^{y,\pm} \in [0, 1]$.

Let $\bar{\omega}$ be some preferable constant value of $\omega_{i,j}^{x,\pm}, \omega_{i,j}^{y,\pm}$, e.g. $\bar{\omega} = 1/3$ as in [23] to achieve the third accurate approximation in space.

Then, setting the weights using the nominators and denominators in \mathbf{r} given in (28)

$$\begin{aligned} a_u^{x,-} &= \bar{\omega} \left(\frac{1}{(\epsilon + (u_{i-1,j}^{n+1} - u_{i,j}^n)^2)^2} \right), & a_u^{y,-} &= \bar{\omega} \left(\frac{1}{(\epsilon + (u_{i,j-1}^{n+1} - u_{i,j}^n)^2)^2} \right), \\ a_c^{x,-} &= (1 - \bar{\omega}) \left(\frac{1}{(\epsilon + (u_{i,j}^{n+1} - u_{i+1,j}^n)^2)^2} \right), & a_c^{y,-} &= (1 - \bar{\omega}) \left(\frac{1}{(\epsilon + (u_{i,j}^{n+1} - u_{i,j+1}^n)^2)^2} \right), \end{aligned} \quad (34)$$

and

$$\begin{aligned} a_u^{x,+} &= \bar{\omega} \left(\frac{1}{(\epsilon + (u_{i+1,j}^{n+1} - u_{i,j}^n)^2)^2} \right), & a_u^{y,+} &= \bar{\omega} \left(\frac{1}{(\epsilon + (u_{i,j+1}^{n+1} - u_{i,j}^n)^2)^2} \right), \\ a_c^{x,+} &= (1 - \bar{\omega}) \left(\frac{1}{(\epsilon + (u_{i,j}^{n+1} - u_{i-1,j}^n)^2)^2} \right), & a_c^{y,+} &= (1 - \bar{\omega}) \left(\frac{1}{(\epsilon + (u_{i,j}^{n+1} - u_{i,j-1}^n)^2)^2} \right), \end{aligned} \quad (35)$$

with ϵ being a small number to avoid a zero division [23], we can construct the weights $\omega_{i,j}^{x,\pm}, \omega_{i,j}^{y,\pm}$ such as

$$\omega_{i,j}^{x,-} = \frac{a_u^{x,-}}{a_u^{x,-} + a_c^{x,-}}, \quad \omega_{i,j}^{y,-} = \frac{a_u^{y,-}}{a_u^{y,-} + a_c^{y,-}}, \quad \omega_{i,j}^{x,+} = \frac{a_u^{x,+}}{a_u^{x,+} + a_c^{x,+}}, \quad \omega_{i,j}^{y,+} = \frac{a_u^{y,+}}{a_u^{y,+} + a_c^{y,+}}. \quad (36)$$

The corrector-predictor procedure for using the WENO scheme is composed of the following steps:

1. Calculate a predicted value ($u_{i,j}^{n+1}$), using the numerical scheme with the given starting value $\omega_{i,j}^{x,\pm} = \omega_{i,j}^{y,\pm} = \bar{\omega}$. The calculation involves performing the fast sweeping method.
2. The corrector consists of (at least) 4GS iterations in prescribed order as given in (25), where for each of the iterations, one needs to perform:
 - 2.1 Calculate the weights $a_{u,c}^{x,\pm}, a_{u,c}^{y,\pm}$ from (34, 35) using the predicted value.
 - 2.2 Set $\omega_{i,j}^{x,\pm}$ and $\omega_{i,j}^{y,\pm}$ with (36) using the weights from the previous step; and, get the values $l_{i,j}^{x,\pm}, l_{i,j}^{y,\pm}$ from (29).
 - 2.3 Calculate the corrected value $u_{i,j}^{n+1}$ using the obtained values $\omega_{i,j}^{x,\pm}, \omega_{i,j}^{y,\pm}$ and $l_{i,j}^{x,\pm}$ and $l_{i,j}^{y,\pm}$.
 - 2.4 Set either the corrected value as a new predictor and perform again Step 2, or accept the corrected values.

5 Numerical experiments

We present numerical results of the proposed second order and high resolution compact implicit finite-volume scheme with the purpose of illustrating their accuracy and stability properties. We describe the results in two subsections, the first one dealing with a linear advection equation, and the second one dealing with a Burgers equation as a simple representative nonlinear problem. For each of the cases, we present an example with a smooth initial condition, as well as an example with a discontinuous initial condition, employing both the ENO and WENO schemes. Specifically for the Burgers equation, we demonstrate two phenomena, shock and rarefaction waves, separately.

If the exact solution is known for chosen example, it is used for boundary conditions, and the discrete L_1 norm (E) of the error is calculated as follows,

$$E = h^2 \sum_{i=1}^M \sum_{j=1}^M |u_{ij}^N - \bar{u}_{ij}^N| \quad (37)$$

Moreover, the Experimental Order of Convergence (EOC) is computed using the errors from (37) to confirm the expected order of the accuracy for the chosen examples. Note that to avoid a reduction of the accuracy due to boundary conditions when computing the EOC, we set exact values not only at the inflow boundary points, but also in a neighboring point outside of the computational interval to use the full stencil of the scheme for every inner grid point. Concerning the time steps, we choose maximal Courant numbers larger than allowed by a stability restriction of explicit schemes to test the stability behavior of the compact implicit schemes.

The numerical methods and the graphical output are obtained using the Python programming language [21].

5.1 Linear advection equation

We compute a linear problem in the form (13). As a guiding factor, we compute the maximal value of Courant number at each direction

$$C_{max}^x = \frac{\tau}{h} \max_{i,j} \{|v_{i+1/2,j}|\}, \quad C_{max}^y = \frac{\tau}{h} \max_{i,j} \{|w_{i,j+1/2}|\},$$

over all edges of each finite volume. These "directional" Courant numbers will be larger than allowed by a stability restriction of explicit schemes.

For the two dimensional experiments we choose the computation domain $x, y \in [-1, 1]$ and the velocity field representing the rotation in the form

$$\vec{v} = (-2\pi y, 2\pi x), \quad (38)$$

which is shown in Figure 2, where the exact solution for any initial function u^0 is defined as

$$u(x, y, t) = u^0(x \cos(2\pi t) + y \sin(2\pi t), y \cos(2\pi t) - x \sin(2\pi t)). \quad (39)$$

In the first example, we consider the initial condition in a form of Gaussian

$$u^0(x, y) = e^{10(-(x-0.25)^2 - (y-0.25)^2)} \quad (40)$$

and in the first experiment, we will choose the final time $T = 0.25$. to speed up the calculation time. In such a case, the Gaussian moves by a quarter of a cycle. The initial condition with the exact solution are shown in Fig. 3.

We computed the experiment for three different (but fixed) choices of ω to show the second order accuracy of the method. We chose sequentially $M = 40, 80, 160, 320$ and 640 , and $N = M/10$ which leads to $C_{max}^x = C_{max}^y = 7.854$. The initial condition together with the contours of the numerical solution are shown in Fig. 5 for different times $t = T/3, 2T/3, T$, with $T = 0.25$. The errors and EOCs in Table 1 confirm the expected order of accuracy for the three different values $\omega^{x,\pm}, \omega^{y,\pm} = 0, 1/2, 1$ used. We also use the ENO and WENO ($\bar{\omega} = 1/3$) schemes to check the order of accuracy for such schemes. We also compute the errors and the EOCs using the first order accurate numerical scheme (18) to show the significant difference in errors when using higher order accurate schemes. For this first experiment, to solve the system of linear algebraic equations, a fast sweeping method with four Gauss-Seidel iterations sufficed.

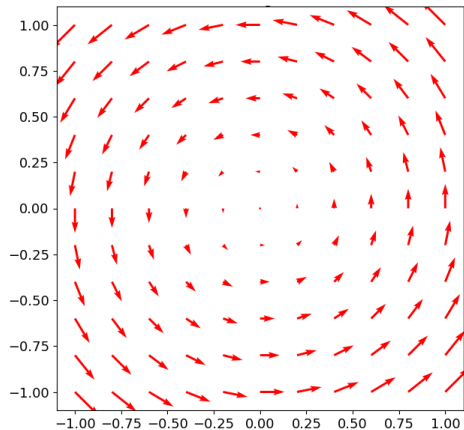


Figure 2: Velocity field in (38).

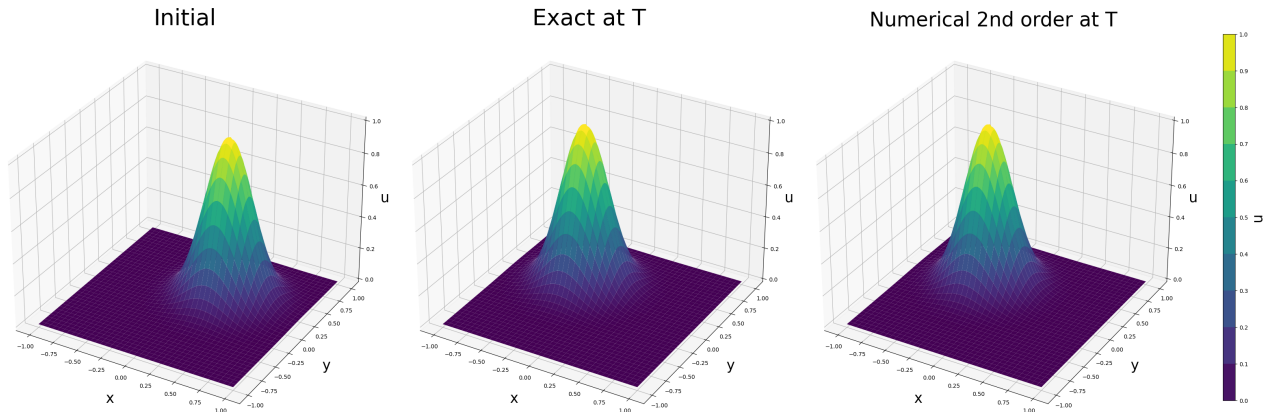


Figure 3: The initial condition, the exact solution and the numerical solution obtained by the second order accurate scheme with $\omega^{x,\pm}, \omega^{y,\pm} = 0$, $M = 320$, $T = 0.25$, only 4 Gauss-Seidel iterations performed.

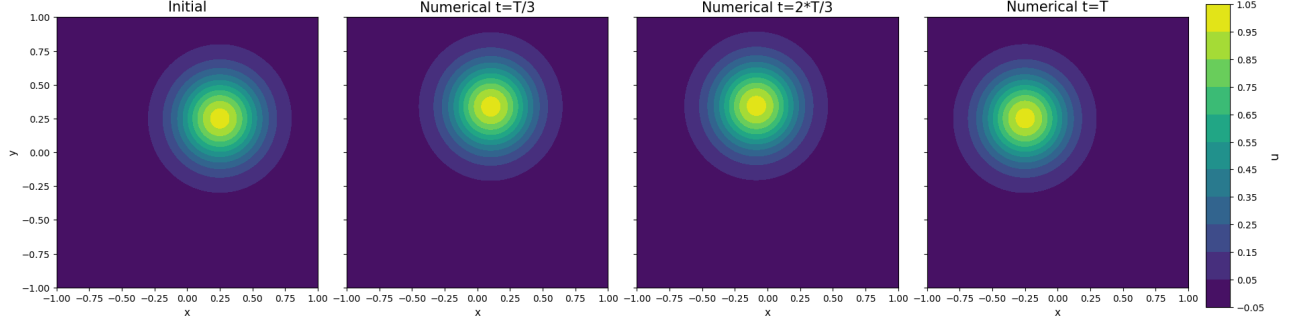


Figure 4: Contours of the numerical solution of the rotation of Gaussian, obtained by the second order accurate scheme with 4GS and $\omega^{x,\pm}, \omega^{y,\pm} = 0$ at different times $t = 0, T/3, 2T/3, T$ with $M = 320$, and with $C_{max}^x = C_{max}^y = 7.854$.

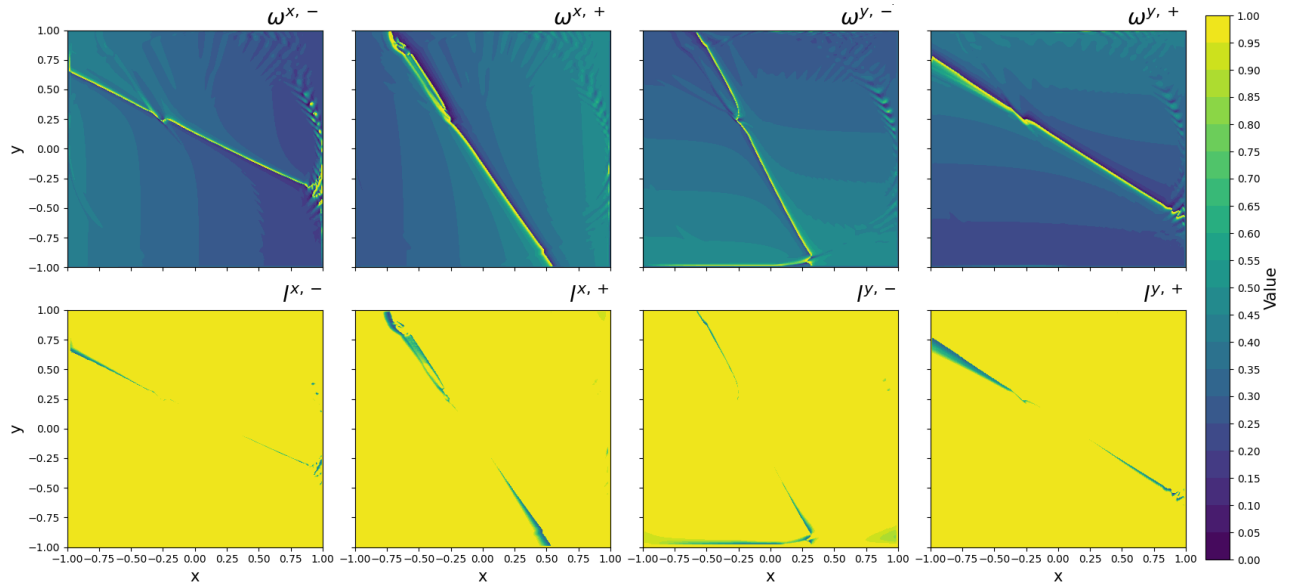


Figure 5: Visualization of ω and l at the final time $T = 0.25$ when using the WENO scheme with 4GS and $\bar{\omega} = 1/3$ for the rotation of Gaussian, $M = 320$, $C_{max}^x = C_{max}^y = 7.854$.

		$\omega^{x,\pm}, \omega^{y,\pm} = 0$			$\omega^{x,\pm}, \omega^{y,\pm} = 1/2$			$\omega^{x,\pm}, \omega^{y,\pm} = 1$		
M	N	E	EOC	max	E	EOC	max	E	EOC	max
40	4	0.06959	-	0.95	0.03687	-	0.95	0.02543	-	0.93
80	8	0.02163	1.68	0.97	0.01087	1.76	0.99	0.00693	1.92	0.98
160	16	0.00578	1.90	0.99	0.00285	1.93	0.99	0.00175	1.98	0.99
320	32	0.00147	1.97	0.99	0.00072	1.98	0.99	0.00043	1.99	0.99
640	64	0.00037	1.99	0.99	0.00018	1.99	0.99	0.00010	1.99	0.99
		ENO			WENO			1st order		
M	N	E	EOC	max	E	EOC	max	E	EOC	max
40	4	0.04917	-	0.81	0.04513	-	0.84	0.15530	-	0.58
80	8	0.01594	1.62	0.91	0.01604	1.49	0.97	0.10447	0.57	0.69
160	16	0.00491	1.69	0.96	0.00472	1.76	0.98	0.06366	0.71	0.80
320	32	0.00136	1.85	0.98	0.00125	1.91	0.99	0.03600	0.82	0.88
640	64	0.00036	1.88	0.99	0.00032	1.95	0.99	0.01932	0.89	0.93

Table 1: The numerical errors and the EOCs of the second order schemes for the rotation of Gaussian, $C_{max}^x = C_{max}^y = 7.854$.

Next, we present numerical results for a non-smooth solution. As an initial condition for $x, y \in [-1, 1]$, we choose four formations in four quadrants, see (41) and Fig. 6. In particular, a Gaussian with a center at $(0.5, 0.5)$ and height 1, a cone with the center at $(-0.5, 0.5)$ with the maximal radius $r_{max} = 0.25$ and the height 1, a half sphere with the center at $(-0.5, -0.5)$ and the maximal radius r_{max} and the height 1, and a circle with a center at $(0.5, -0.5)$ with radius r_{max} with the value 1 inside the circle and the value 0 everywhere else.

$$u^0(x, y) = \begin{cases} e^{100(-(x-0.5)^2-(y-0.5)^2)} & \text{if } x \geq 0 \text{ and } y \geq 0 \text{ and } (x-0.5)^2 + (y-0.5)^2 < 0.3^2, \\ 1 - \frac{\sqrt{(x+0.5)^2+(y-0.5)^2}}{0.25} & \text{if } x < 0 \text{ and } y \geq 0 \text{ and } \sqrt{(x+0.5)^2 + (y-0.5)^2} \leq 0.25, \\ \sqrt{1 - \left(\frac{\sqrt{(x+0.5)^2+(y+0.5)^2}}{0.25}\right)^2} & \text{if } x < 0 \text{ and } y < 0 \text{ and } \sqrt{(x+0.5)^2 + (y+0.5)^2} \leq 0.25, \\ 1 & \text{if } x \geq 0 \text{ and } y < 0 \text{ and } \sqrt{(x-0.5)^2 + (y+0.5)^2} \leq 0.25, \\ 0 & \text{otherwise.} \end{cases} \quad (41)$$

The velocity field is the same as in (38), and we choose the final time $T = 0.25$ for which the initial condition rotates by a quarter of a circle and the exact solution is obtained using (39). The initial condition and the final solution are shown in Figure 6. We choose $M = 40, 80, 160, 320, 640$ and $N = M/10$ time steps, leading to $C_{max}^x = C_{max}^y = 7.854$.

This time, it is necessary to use the ENO and WENO ($\bar{\omega} = 1/3$) schemes to suppress oscillations in numerical solutions. The errors and the EOCs are shown in Table 2 for the entire computational domain. The differences in the errors for 4 and 8 GS iterations are shown to show rather negligible differences. The Table also contains the comparison to the errors when using the first order accurate scheme. Moreover, in Table 3, the errors and the EOCs are displayed for each sector separately, showing the convergence of each of the formations in the initial condition using the 4 and 8 GS iterations.

		ENO, 4GS		WENO, 4GS		ENO, 8GS		WENO, 8GS		1st order	
M	N	E	EOC	E	EOC	E	EOC	E	EOC	E	EOC
40	4	0.48031	-	0.45872	-	0.47765	-	0.45959	-	0.56302	-
80	8	0.32450	0.56	0.30956	0.56	0.32022	0.57	0.29833	0.62	0.53127	0.08
160	16	0.18626	0.80	0.18315	0.75	0.18285	0.80	0.17129	0.80	0.45594	0.22
320	32	0.10187	0.87	0.10120	0.85	0.09987	0.87	0.09414	0.86	0.35630	0.35
640	64	0.05768	0.82	0.05749	0.81	0.05624	0.83	0.05353	0.81	0.25809	0.46

Table 2: The numerical errors and the EOCs for the ENO and WENO schemes, the example of the rotation of a discontinuous function (41) with $T = 0.25$ over entire computational domain, $C_{max}^x = C_{max}^y = 7.854$.

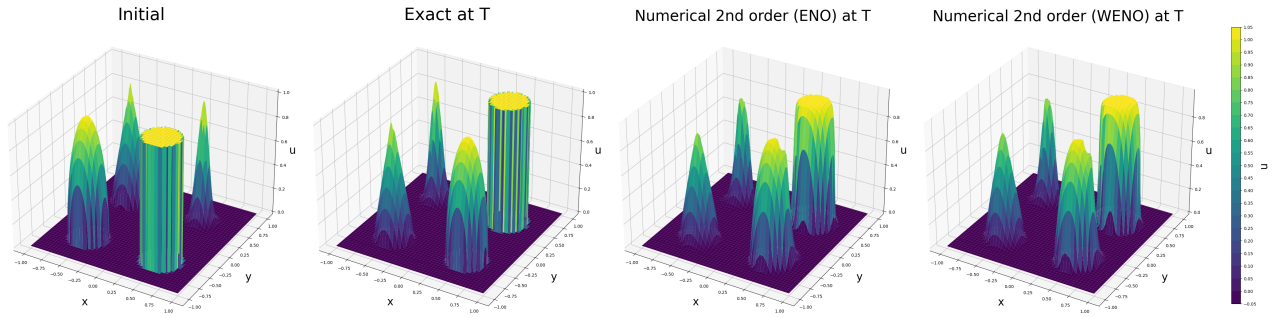


Figure 6: The initial condition and the exact solution for the example of the rotation of (41) with $M = 640$, and numerical results using the ENO and WENO schemes with 8GS.

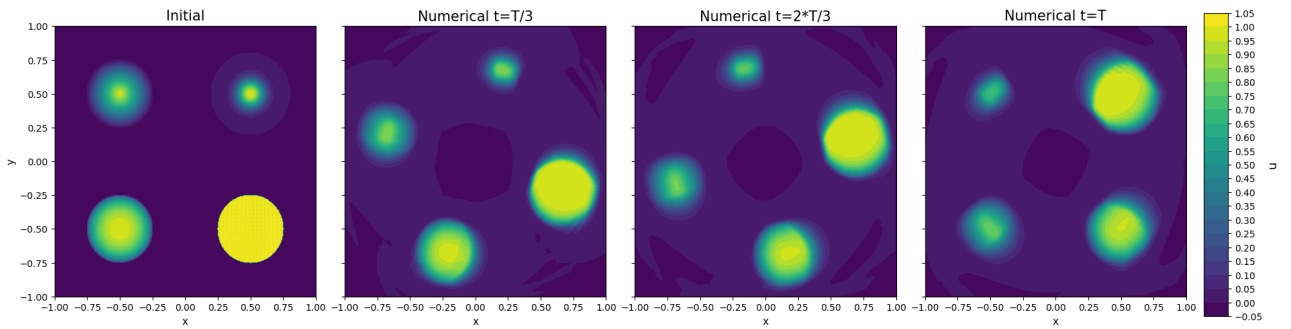


Figure 7: The numerical solution for the example of the rotation of (41) at three times $t = 0, T/3, 2T/3, T$ and $T = 0.25$ obtained using the ENO (8GS) scheme, $M = 320$, $C_{max}^x = C_{max}^y = 7.854$.

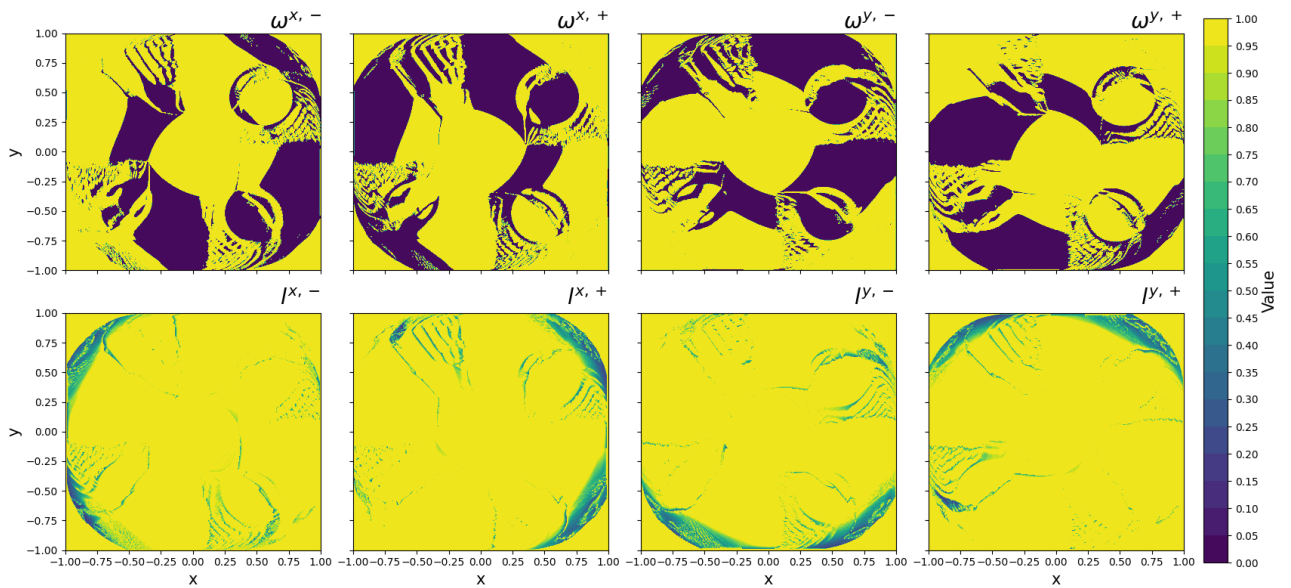


Figure 8: The visualizations of the values of ω and l at $T = 0.25$ obtained using the ENO (8GS) scheme for the rotation of (41), $M = 320$, $C_{max}^x = C_{max}^y = 7.854$.

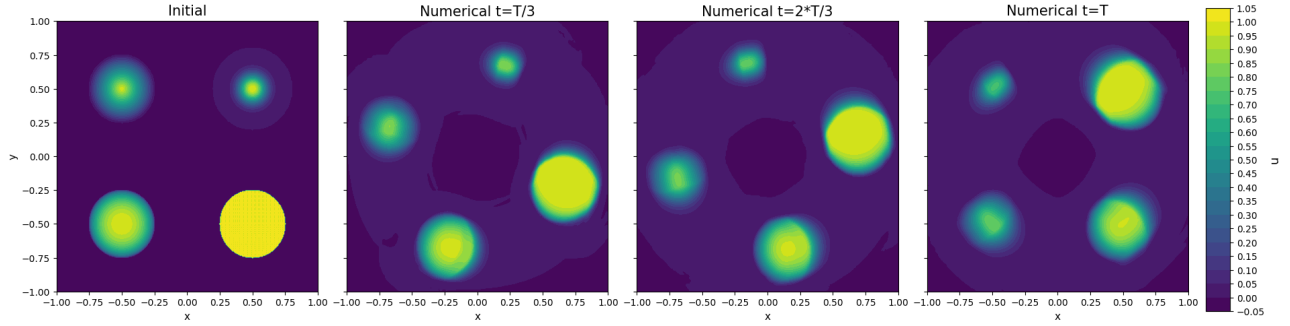


Figure 9: The numerical solution for the example of the rotation of (41) at three times $t = 0, T/3, 2T/3, T$ and $T = 0.25$ obtained using the WENO (8GS) scheme, $M = 320$, $C_{max}^x = C_{max}^y = 7.854$.

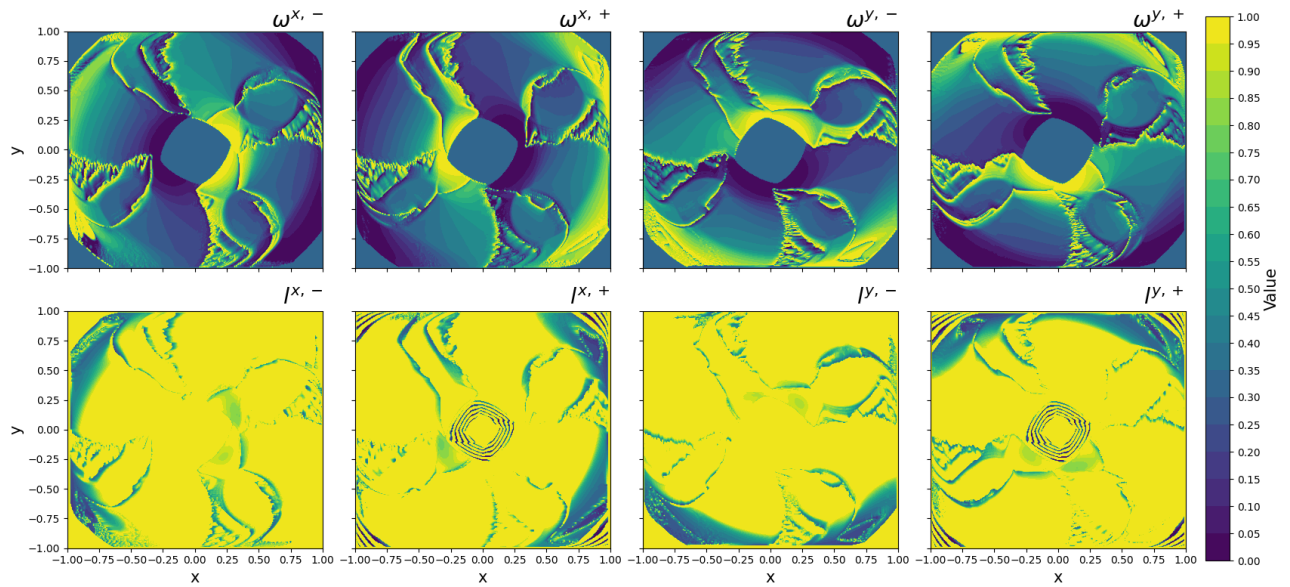


Figure 10: The visualizations of the values of ω and l at $T = 0.25$ obtained using the WENO (8GS) scheme for the rotation of (41), $M = 320$, $C_{max}^x = C_{max}^y = 7.854$.

ENO, 4GS									
		Gaussian		Cone		Half sphere		Circle	
M	N	E	EOC	E	EOC	E	EOC	E	EOC
80	8	0.03482	-	0.04953	-	0.09152	-	0.09152	-
160	16	0.01985	0.81	0.02453	1.01	0.04660	0.97	0.04660	0.64
320	32	0.00924	1.10	0.00989	1.31	0.02229	1.06	0.02229	0.65
640	64	0.00378	1.28	0.00408	1.27	0.01170	0.92	0.01170	0.66
WENO, 4GS									
		Gaussian		Cone		Half sphere		Circle	
M	N	E	EOC	E	EOC	E	EOC	E	EOC
80	8	0.03345	-	0.05008	-	0.08574	-	0.14028	-
160	16	0.02041	0.71	0.02651	0.91	0.04503	0.92	0.09118	0.62
320	32	0.01008	1.01	0.01080	1.29	0.02203	1.03	0.05827	0.64
640	64	0.00424	1.24	0.00454	1.24	0.01177	0.90	0.03692	0.65
ENO, 8GS									
		Gaussian		Cone		Half sphere		Circle	
M	N	E	EOC	E	EOC	E	EOC	E	EOC
80	8	0.03456	-	0.04850	-	0.09029	-	0.14686	-
160	16	0.01955	0.82	0.02371	1.00	0.04601	0.97	0.09356	0.65
320	32	0.00902	1.11	0.00960	1.30	0.02222	1.04	0.05901	0.66
640	64	0.00365	1.30	0.00396	1.27	0.01171	0.92	0.03691	0.68
WENO, 8GS									
		Gaussian		Cone		Half sphere		Circle	
M	N	E	EOC	E	EOC	E	EOC	E	EOC
80	8	0.04764	-	0.04600	-	0.08303	-	0.13693	-
160	16	0.01846	0.80	0.02277	1.01	0.04201	0.98	0.08804	0.63
320	32	0.00867	1.08	0.00937	1.28	0.02040	1.04	0.05569	0.66
640	64	0.00386	1.16	0.00398	1.23	0.01086	0.90	0.03482	0.68

Table 3: The numerical errors and the EOCs for the ENO and WENO schemes, each quadrant separately, the example of the rotation of (41) with $T = 0.25$, $C_{max}^x = C_{max}^y = 7.854$.

5.2 Burgers equation

We compute a representative nonlinear problem in the form of the Burgers equation,

$$\partial_t u + \partial_x \left(\frac{u^2}{2} \right) + \partial_y \left(\frac{u^2}{2} \right) = 0. \quad (42)$$

In this case, the maximum Courant number is defined as $C_{max} = \frac{\tau}{h} u_{max}$, with $u_{max} = \max(|u_{i,j}^n|)$ over all time steps and finite volumes.

For the first 2D example we choose the computation domain $x, y \in [-1, 1]$ and $t \in [0, 0.5]$ with a smooth initial condition (Fig. 11) in the form

$$u^0(x, y) = \sin(\pi x) \sin(\pi y) / 2. \quad (43)$$

The exact solution can be obtained numerically using the method of characteristics by solving the algebraic equations for $u = u(x_i, y_j, t^n)$

$$u = \sin(\pi(x_i - ut^n)) \sin(\pi(y_j - ut^n)) / 2. \quad (44)$$

For this example, we chose sequentially $M = 80, 160, 320$ and 640 , and the number of time steps is $N = M/80$. Together with the maximum absolute value of the function u^0 being 0.5 , one obtains $C_{max} = 10$.

We show results using the compact implicit numerical scheme with the constant values of $\omega^{x,\pm}, \omega^{y,\pm} = 0, 1/2, 1$, sequentially. We compute the errors (37) in the final time $T = 0.5$, the EOC and also the minimum and maximum value of u . The errors and the EOCs in Table 4 confirm the expected order of accuracy for the different values $\omega^{x,\pm}, \omega^{y,\pm}$. We also show results using the ENO and WENO (with $\bar{\omega} = 1/3$) schemes, to demonstrate the order of accuracy. Notice that the maximum and minimum values when using the ENO and WENO schemes keep values of u within the limits, unlike the constant value of ω used everywhere else. The results can be compared with the errors of the first order accurate scheme in Table 4. The visualization of the choice of ω and \mathbf{l} for the ENO and WENO schemes are shown in Figures 13, 14, respectively.

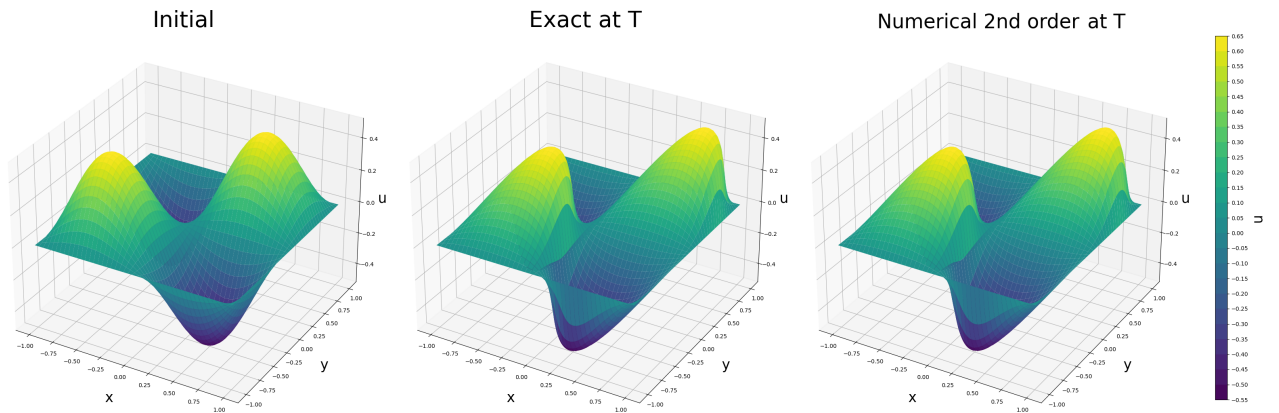


Figure 11: The initial condition (left), the exact solution (middle) and the numerical solution (right) obtained by the second order scheme at $T = 0.5$ using 4GS for the nonlinear problem with the smooth initial condition (43), $\omega^{x,\pm}, \omega^{y,\pm} = 1$, $M = 320$.

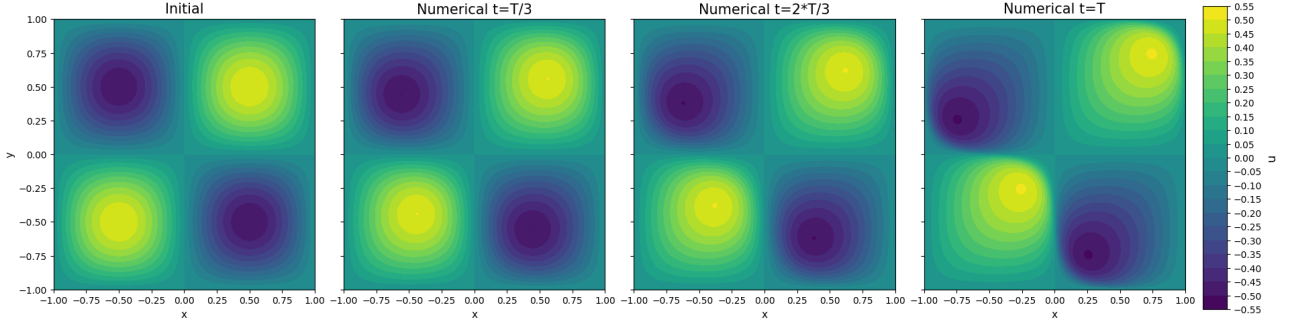


Figure 12: Contours of the numerical solution of the nonlinear problem with the smooth initial condition (43) obtained by the second order accurate numerical scheme (4GS) at times $t = 0, T/3, 2T/3, T$ with $T = 0.5$, $M = 320$, $\omega^{x,\pm}, \omega^{y,\pm} = 1$, $C_{max} = 10$.

		$\omega^{x,\pm}, \omega^{y,\pm} = 0$				$\omega^{x,\pm}, \omega^{y,\pm} = 1/2$				$\omega^{x,\pm}, \omega^{y,\pm} = 1$			
M	N	E	EOC	min	max	E	EOC	min	max	E	EOC	min	max
80	1	0.0599	-	-0.510	0.510	0.0516	-	-0.508	0.508	0.0436	-	-0.503	0.503
160	2	0.0247	1.27	-0.505	0.505	0.0209	1.29	-0.504	0.504	0.0175	1.31	-0.506	0.506
320	4	0.0083	1.56	-0.501	0.501	0.0069	1.59	-0.501	0.501	0.0057	1.61	-0.503	0.503
640	8	0.0024	1.78	-0.500	0.500	0.0019	1.80	-0.500	0.500	0.0016	1.83	-0.501	0.501

		ENO				WENO				1st order			
M	N	E	EOC	min	max	E	EOC	min	max	E	EOC	min	max
80	1	0.0603	-	-0.460	0.460	0.0590	-	-0.460	0.460	0.1323	-	-0.417	0.417
160	2	0.0255	1.23	-0.478	0.478	0.0250	1.23	-0.477	0.477	0.0918	0.52	-0.433	0.433
320	4	0.0082	1.63	-0.489	0.489	0.0080	1.62	-0.489	0.489	0.0595	0.62	-0.453	0.453
640	8	0.0023	1.83	-0.497	0.496	0.0022	1.82	-0.496	0.496	0.0357	0.73	-0.470	0.470

Table 4: The numerical errors, the EOCs and the minimum and maximum values for the first and second order schemes computed for the nonlinear problem with the smooth initial condition (43), $T = 0.5$, $C_{max} = 10$.

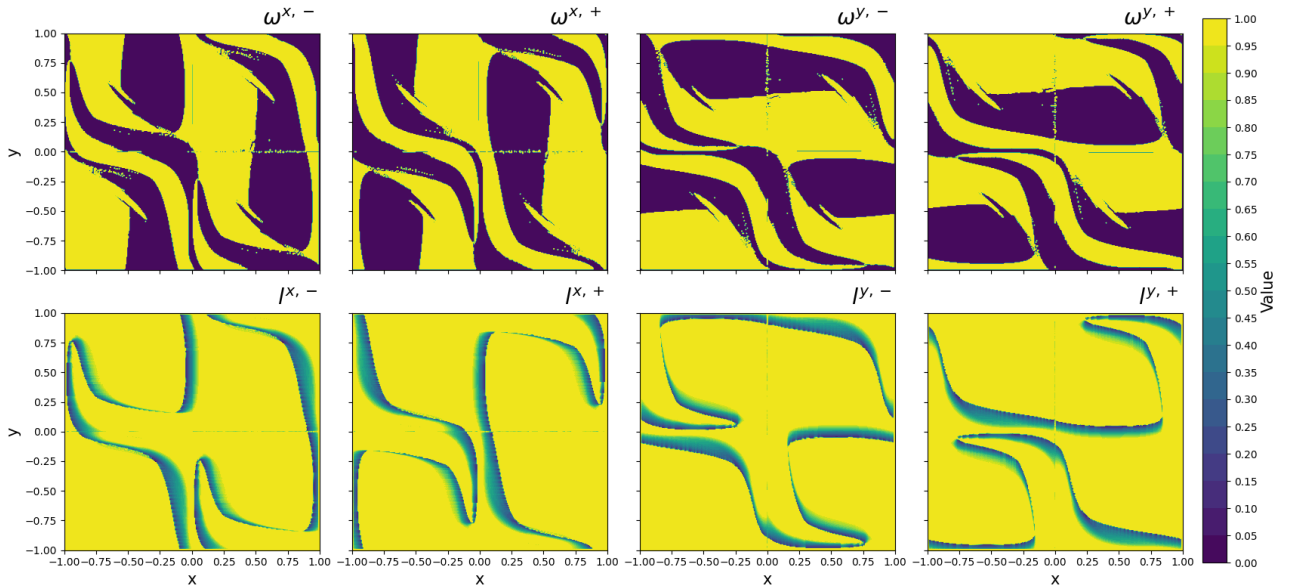


Figure 13: The visualizations of the values of ω and l at time $T = 0.4$ obtained using the ENO (4GS) scheme for the smooth initial conditions (43), $M = 320$, $C_{max} = 10$.

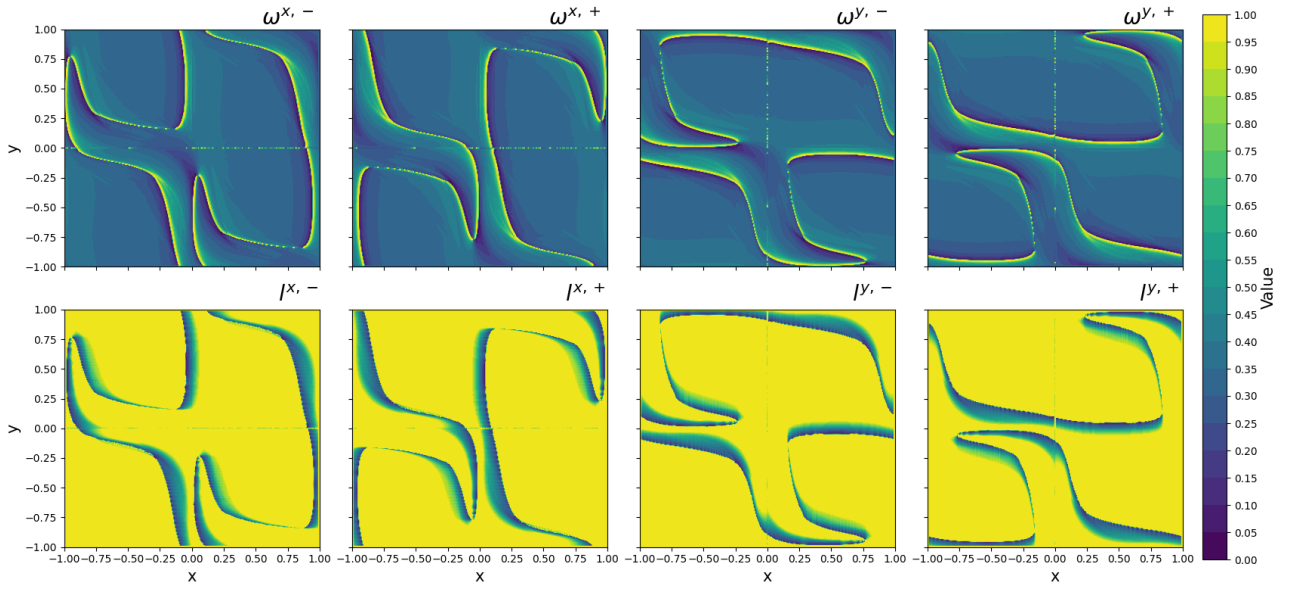


Figure 14: The visualizations of the values of ω and l at time $T = 0.4$ obtained using the WENO (4GS) scheme with the initial condition (43), $M = 320$, $C_{max} = 10$.

The second problem is, again, defined for $x, y \in [-1, 1]$ and will consider a rarefaction wave effect. The initial condition (Figure 15) is given in the form

$$u^0(x, y) = \begin{cases} u_L & \text{if } \frac{x+y}{2} < 0 \\ u_R & \text{otherwise} \end{cases}, \quad (45)$$

for $u_L = -1$ and $u_R = 1$; and, the exact solution is prescribed as

$$u(x, y, t) = \begin{cases} u_L & \text{if } \frac{x+y}{2} \leq -t \\ \frac{x+y}{2t} & \text{if } -t < \frac{x+y}{2} \leq t \\ u_R & \text{if } \frac{x+y}{2} > t \end{cases}, \quad (46)$$

and we will compute the solution for $t \in [0, 0.4]$.

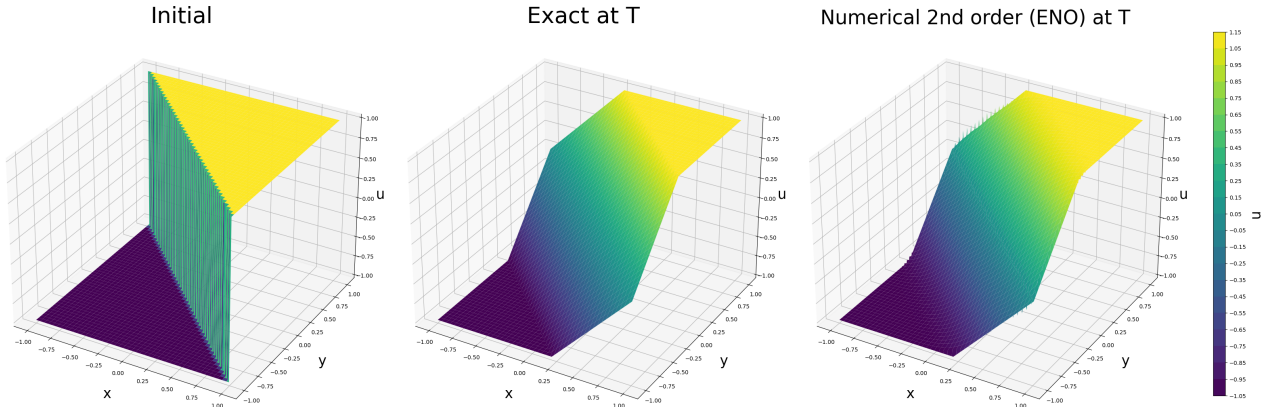


Figure 15: The initial condition (left), the exact solution (middle) and the numerical solution (right) obtained by the ENO (8GS) scheme at $T = 0.4$, $M = 320$ for the nonlinear problem with the initial condition (46).

This time we choose $N = M/40$ number of time steps for $M = 80, 160, 320, 640$, with the value $C_{max} = 8$. The ENO and WENO (with $\bar{\omega} = 1/3$) schemes were used to compute the solution, together with the first order accurate scheme, to demonstrate the difference in the errors obtained for 4 and 8 GS iterations, see Table 5.

		ENO, 4GS		WENO, 4GS		ENO, 8GS		WENO, 8GS		1st order	
M	N	E	EOC	E	EOC	E	EOC	E	EOC	E	EOC
80	2	0.34522	-	0.33213	-	0.33366	-	0.30509	-	0.49101	-
160	4	0.18866	0.87	0.17907	0.89	0.18425	0.85	0.16846	0.85	0.35488	0.46
320	8	0.09926	0.92	0.09331	0.94	0.09734	0.92	0.08890	0.92	0.24549	0.53
640	16	0.05096	0.96	0.04756	0.97	0.05008	0.95	0.04565	0.96	0.16124	0.60

Table 5: The numerical errors and the EOCs for the first and second (ENO, WENO) order accurate schemes for the nonlinear problem with the initial condition shown in Figure 15, $T = 0.4$, $C_{max} = 8$.

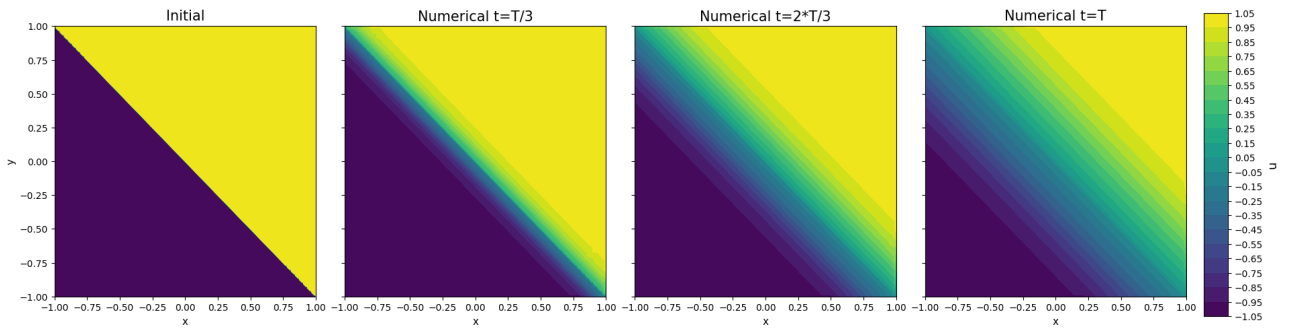


Figure 16: Numerical solution at three time steps $t = 0, T/3, 2T/3, T$, for $T = 0.4$ obtained using the second order ENO (8GS) scheme, $M = 320$, $C_{max} = 8$.

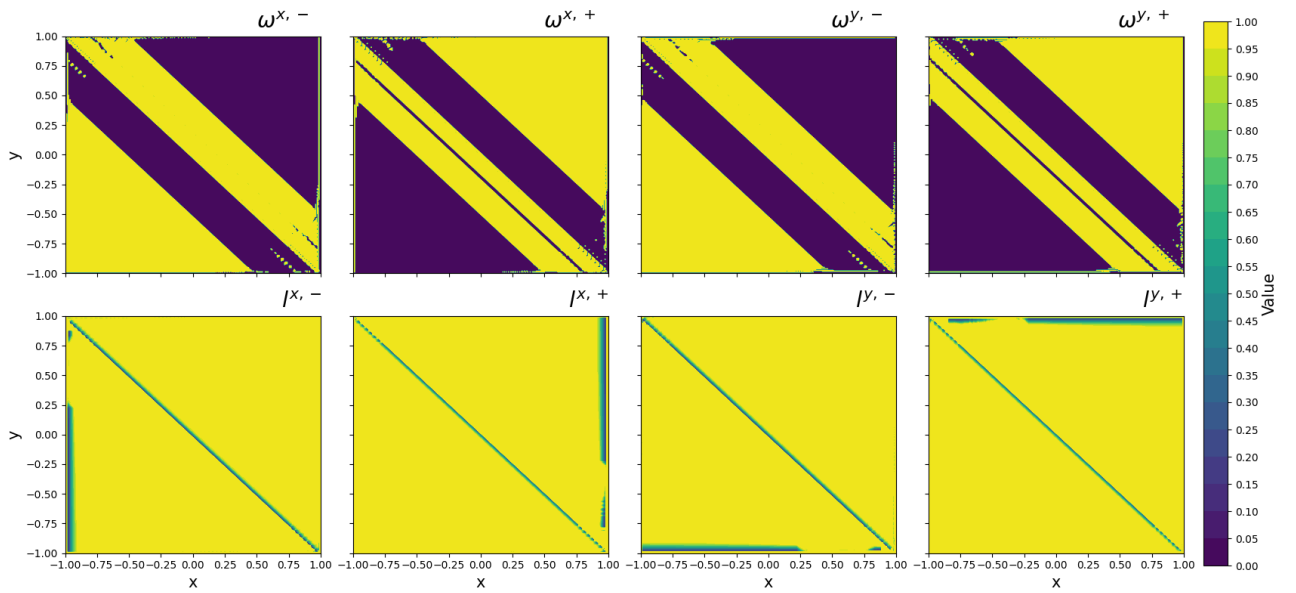


Figure 17: The visualizations of the values of ω and l at time $T = 0.4$ obtained using the ENO (8GS) scheme, $M = 320$, $C_{max} = 8$.

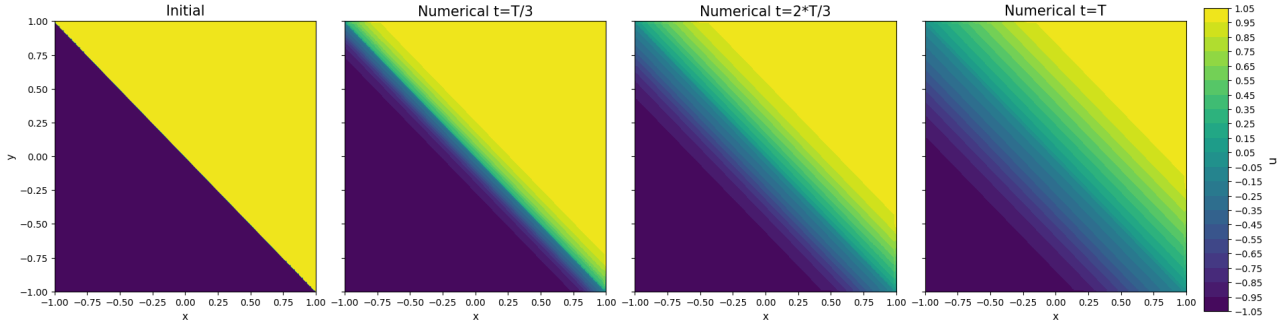


Figure 18: Numerical solution at three time steps $t = 0, T/3, 2T/3, T$, for $T = 0.4$ obtained using the second order WENO (8GS) scheme, $M = 320, C_{max} = 8$.

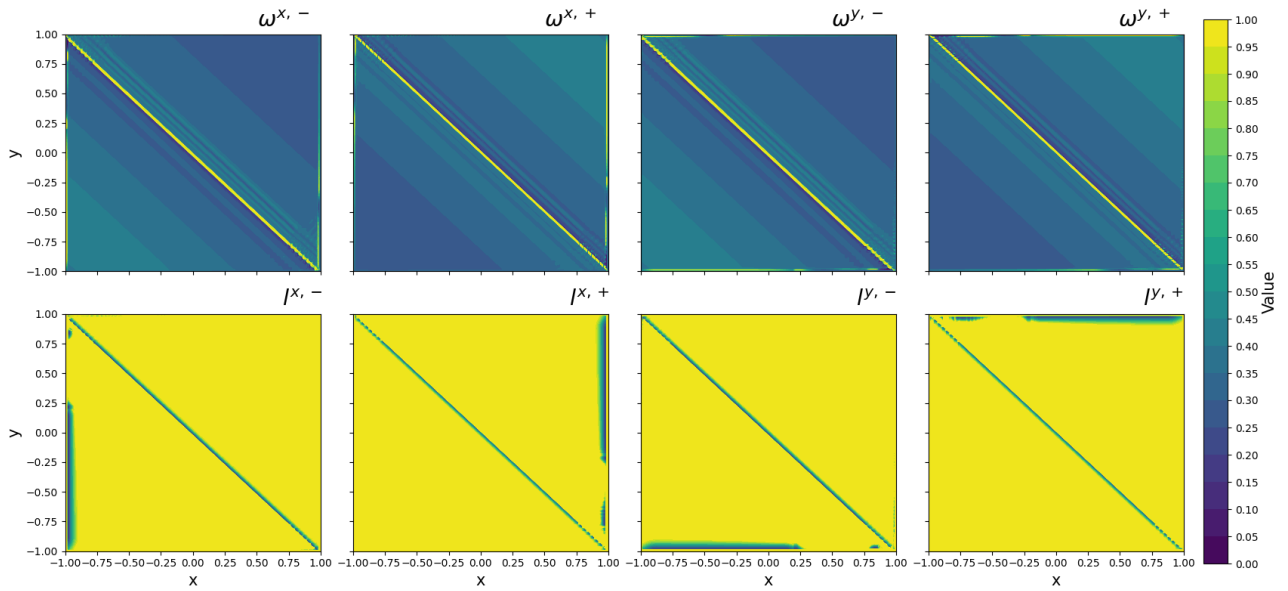


Figure 19: The visualizations of the values of ω and l at time $T = 0.4$ obtained using the WENO (8GS) scheme, $M = 320, C_{max} = 8$.

The last problem deals with a discontinuity in the form of a shock wave and will be defined for $x, y \in [-1, 1]$ with the computational time $t \in [0, 0.4]$. The initial condition in Figure 20 is given in the form

$$u^0(x, y) = \begin{cases} u_{L1} & \text{if } x < -0.8 \text{ or } y < -0.8 \text{ or } x + y < -0.8 \\ u_{L2} & \text{if } x < 0.2 \text{ or } y < 0.2 \text{ or } x + y < 0.7 \\ u_{R2} & \text{otherwise} \end{cases}, \quad (47)$$

with $u_{L1} = 1$, $u_{R1} = u_{L2} = 0.1$ and $u_{R2} = -0.5$, and the exact solution is prescribed as

$$u(x, y, t) = \begin{cases} u_{L1} & \text{if } x < -0.8 + s_{x1}t \text{ or } y < -0.8 + s_{y1}t \text{ or } x + y < -0.8 + (s_{x1} + s_{y1})t \\ u_{L2} & \text{if } x < 0.2 + s_{x2}t \text{ or } y < 0.2 + s_{y2}t \text{ or } x + y < 0.7 + (s_{x2} + s_{y2})t \\ u_{R2} & \text{otherwise} \end{cases}, \quad (48)$$

with s_{x1}, s_{x2}, s_{y1} and s_{y2} being the shock speeds

$$\begin{aligned} s_{x1} &= \frac{f(u_{L1}) - f(u_{R1})}{u_{L1} - u_{R1}}, & s_{x2} &= \frac{f(u_{L2}) - f(u_{R2})}{u_{L2} - u_{R2}}, \\ s_{y1} &= \frac{g(u_{L1}) - g(u_{R1})}{u_{L1} - u_{R1}}, & s_{y2} &= \frac{g(u_{L2}) - g(u_{R2})}{u_{L2} - u_{R2}}. \end{aligned} \quad (49)$$

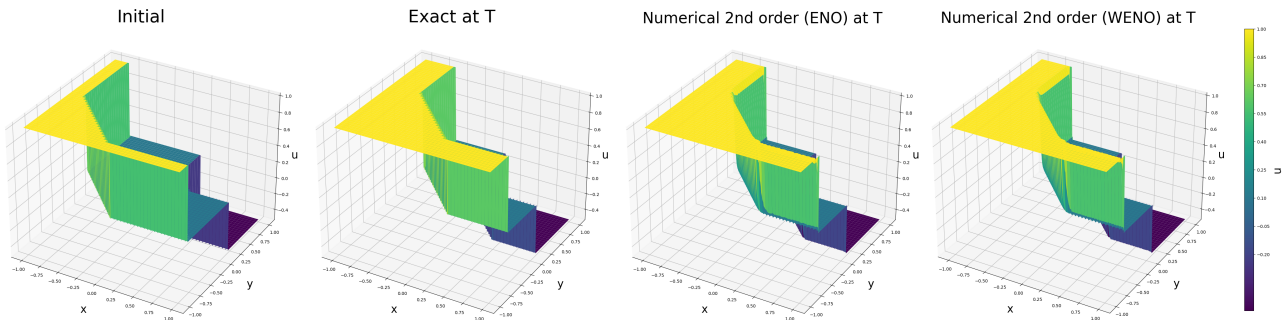


Figure 20: The visualization of the initial condition (left), the exact solution (second left) and the the numerical solutions (right) obtained by the ENO and WENO (8GS) schemes at $T = 0.4$, $M = 320$ for the nonlinear problem with the initial condition (47).

Again, we choose $N = M/40$ number of time steps for $M = 80, 160, 320, 640$, with the value $C_{max} = 8$. The ENO and WENO ($\bar{\omega} = 1/3$) schemes were used to compute the solution, using 4 and 8 GS iterations, together with the first order accurate scheme, to demonstrate the difference in the errors obtained, see Table 6. This time, it was useful to perform the eight Gauss-Seidel iterations, especially when using the ENO approximations, to obtain a better accuracy and convergence.

M	N	ENO, 4GS		WENO, 4GS		ENO, 8GS		WENO, 8GS		1st order	
		E	EOC	E	EOC	E	EOC	E	EOC	E	EOC
80	2	0.11936	-	0.11909	-	0.12562	-	0.12392	-	0.25841	-
160	4	0.06354	0.90	0.06341	0.90	0.06609	0.92	0.06534	0.92	0.15270	0.75
320	8	0.03547	0.84	0.03330	0.92	0.03411	0.95	0.03377	0.95	0.08418	0.85
640	16	0.02033	0.80	0.01721	0.95	0.01720	0.98	0.01704	0.98	0.04341	0.95

Table 6: The numerical errors and the EOCs for the first and second (ENO, WENO) order accurate schemes for the nonlinear problem with the initial condition shown in Figure 20, $T = 0.4$, $C_{max} = 8$.

6 Conclusion

In this paper, we derived the second order accurate compact implicit numerical schemes in two dimensions for solving hyperbolic problems in the form of scalar conservation laws. Our approach utilizes the finite volume

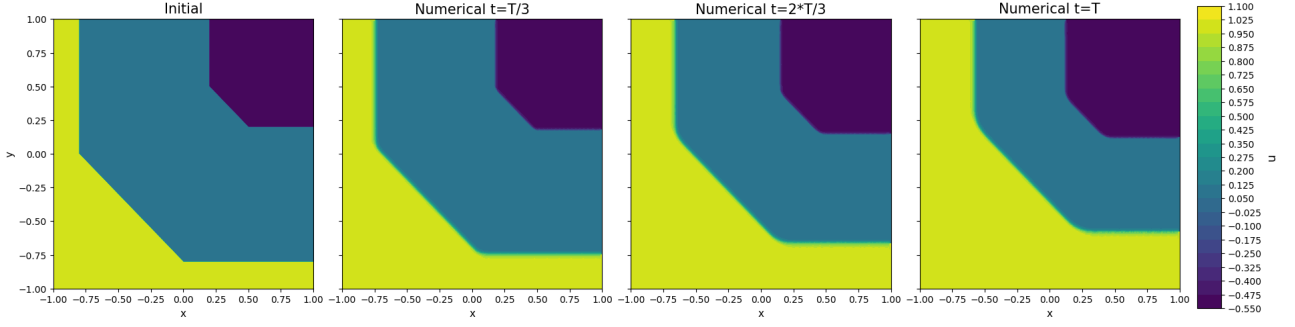


Figure 21: Numerical solutions at three times $t = 0, T/3, 2T/3, T$ for $T = 0.4$ obtained using the ENO (8GS) scheme for the example with shocks, $M = 320$, $C_{max} = 8$.

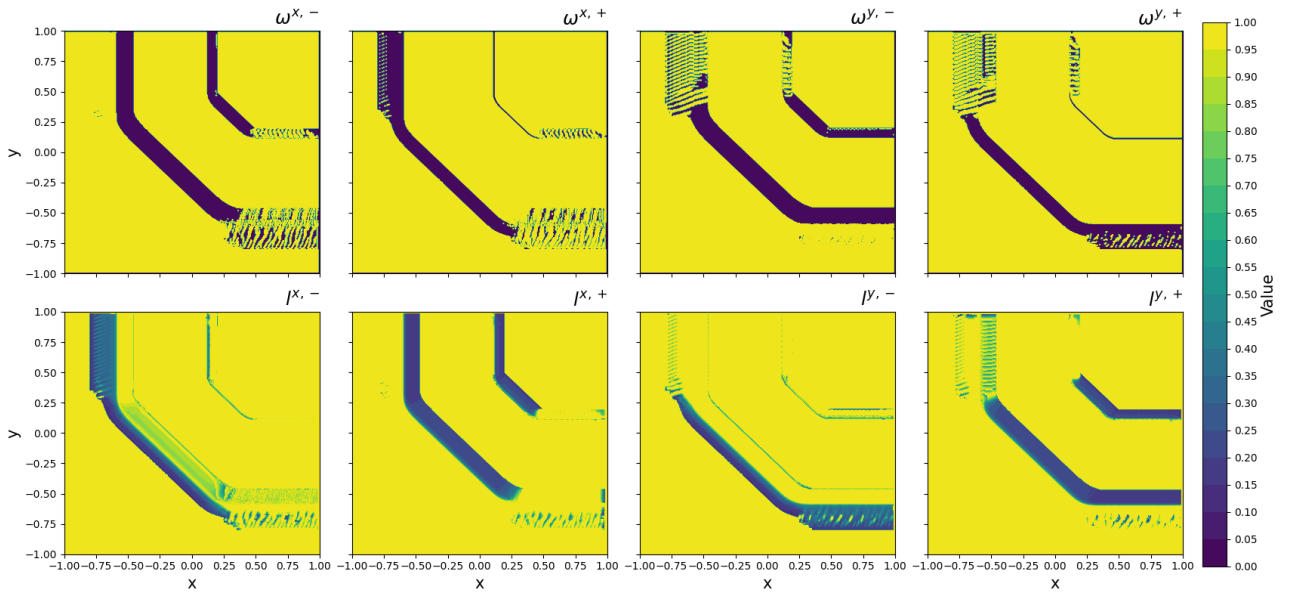


Figure 22: The visualizations of the values of ω and l at time $T = 0.4$ obtained using the ENO (8GS) scheme for the example with shocks, $M = 320$, $C_{max} = 8$.

method, leveraging the compactness of the stencil for computational efficiency. The solution can be efficiently obtained through the fast sweeping method combined with nonlinear Gauss-Seidel iterations.

The parametric form of our second order scheme inherently supports the use of Essentially Non-Oscillatory (ENO) and Weighted Essentially Non-Oscillatory (WENO) schemes [23] for handling discontinuous solutions. By appropriately choosing the parameters in ω and l , the approximation can be effectively limited in both space and time [10], mitigating oscillations in the numerical solutions through the corresponding predictor-corrector procedure.

We validated these schemes through numerical experiments on selected examples of linear and nonlinear scalar conservation laws demonstrating their properties in various scenarios.

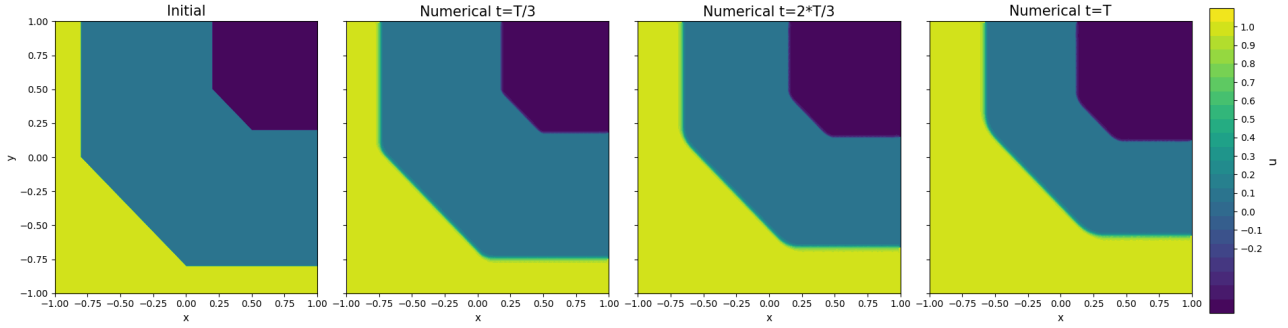


Figure 23: Numerical solutions at three times $t = 0, T/3, 2T/3, T$, for $T = 0.4$ obtained using the WENO (8GS) scheme for the example with shocks, $M = 320$, $C_{max} = 8$.

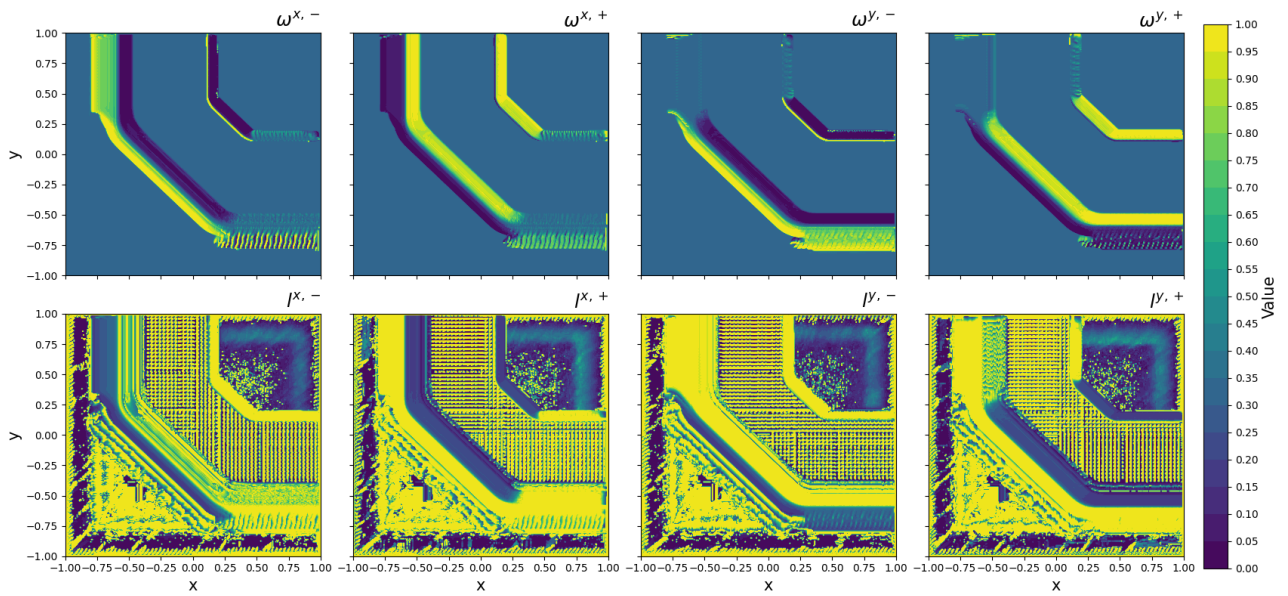


Figure 24: The visualizations of the values of ω and l at time $T = 0.4$ obtained using the WENO (8GS) scheme for the example with shocks, $M = 320$, $C_{max} = 8$.

References

- [1] Todd Arbogast et al. “A third order, implicit, finite volume, adaptive Runge–Kutta WENO scheme for advection–diffusion equations”. In: *Comput. Meth. Appl. Mech. Eng.* (2020).
- [2] Sebastiano Boscarino, Francis Filbet, and Giovanni Russo. “High Order Semi-implicit Schemes for Time Dependent Partial Differential Equations”. In: *J Sci Comput* (Sept. 2016).
- [3] Sebastiano Boscarino and Giovanni Russo. “On a class of uniformly accurate IMEX Runge–Kutta schemes and applications to hyperbolic systems with relaxation”. In: *SIAM Journal on Scientific Computing* (2009).
- [4] Sebastiano Boscarino et al. “Linearly implicit IMEX Runge–Kutta methods for a class of degenerate convection-diffusion problems”. In: *SIAM Journal on Scientific Computing* 37.2 (2015), B305–B331.
- [5] Hugo Carrillo and Carlos Parés. “Compact approximate Taylor methods for systems of conservation laws”. In: *Journal of Scientific Computing* (2019).
- [6] Hugo Carrillo, Carlos Parés, and David Zorío. “Lax-Wendroff approximate Taylor methods with fast and optimized weighted essentially non-oscillatory reconstructions”. In: *Journal of Scientific Computing* (2021).
- [7] Karthikeyan Duraisamy and James D. Baeder. “Implicit Scheme for Hyperbolic Conservation Laws Using Nonoscillatory Reconstruction in Space and Time”. In: *SIAM J. Sci. Comput.* 29.6 (2007).
- [8] Peter Frolkovič. “Maximum principle and local mass balance for numerical solutions of transport equation coupled with variable density flow”. In: *Acta Mathematica Universitatis Comenianae* 1.68 (1998), pp. 137–157.
- [9] Peter Frolkovič and Karol Mikula. “Semi-implicit second order schemes for numerical solution of level set advection equation on Cartesian grids”. In: *Appl. Num. Math.* (2018).
- [10] Peter Frolkovič and Michal Žeravý. “High resolution compact implicit numerical scheme for conservation laws”. In: *Applied Mathematics and Computation* (2023).
- [11] Peter Frolkovič et al. “Semi-implicit methods for advection equations with explicit forms of numerical solution”. In: *Japan J. Indust. Appl. Math.* 39.3 (Dec. 2022).
- [12] Sigal Gottlieb et al. “High Order Strong Stability Preserving MultiDerivative Implicit and IMEX Runge–Kutta Methods with Asymptotic Preserving Properties”. In: *SIAM J. Numer. Anal.* 60.1 (Feb. 2022).
- [13] Friedemann Kemm. “A comparative study of TVD-limiters—well-known limiters and an introduction of new ones”. In: *International Journal for Numerical Methods in Fluids* (2011).
- [14] Randall J Leveque. *Finite Volume Methods for Hyperbolic Problems*. en. 2nd. Cambridge UP, 2004.
- [15] Jiequan Li. “Two-stage fourth order: temporal-spatial coupling in computational fluid dynamics (CFD)”. In: *Adv. Aerodyn.* 1 (Feb. 2019), p. 3.
- [16] Eduardo Lozano and Tariq D. Aslam. “Implicit fast sweeping method for hyperbolic systems of conservation laws”. In: *J. Comp. Phys.* 430 (Apr. 2021).
- [17] Victor Michel-Dansac and Andrea Thomann. “TVD-MOOD schemes based on implicit-explicit time integration”. In: *Applied Mathematics and Computation* (2022).
- [18] Lorenzo Pareschi and Giovanni Russo. “Implicit–explicit Runge–Kutta schemes and applications to hyperbolic systems with relaxation”. In: *Journal of Scientific computing* (2005).
- [19] G. Puppo, M. Semplice, and G. Visconti. “Quinpi: Integrating Conservation Laws with CWENO Implicit Methods”. In: *Commun. Appl. Math. Comput.* (Feb. 2022). ISSN: 2661-8893.
- [20] Jianxian Qiu and Chi-Wang Shu. “Finite Difference WENO Schemes with Lax–Wendroff-Type Time Discretizations”. In: *SIAM J. Sci. Comp.* 24 (May 2003).
- [21] G. van Rossum. *Python tutorial*. Tech. rep. Centrum voor Wiskunde en Informatica (CWI), May 1995.
- [22] David C. Seal, Yaman Güçlü, and Andrew J. Christlieb. “High-Order Multiderivative Time Integrators for Hyperbolic Conservation Laws”. In: *J. Sci. Comput.* (July 2014).
- [23] Chi-Wang Shu. “Essentially non-oscillatory and weighted essentially non-oscillatory schemes for hyperbolic conservation laws”. In: *Advanced Numerical Approximation of Nonlinear Hyperbolic Equations*. Lecture Notes in Mathematics. Berlin, Heidelberg: Springer, 1998.
- [24] Angela Y. J. Tsai, Robert P. K. Chan, and Shixiao Wang. “Two-derivative Runge–Kutta methods for PDEs using a novel discretization approach”. In: *Numer. Alg.* (Mar. 2014).

- [25] Dagmar Zakova. “Second order accurate compact implicit numerical scheme for solving linear advection equation in two dimensions”. In: *Advances in architectural, civil and environmental engineering 33rd annual PhD student conference on applied mathematics, building technology, geodesy and cartography, landscaping, theory and environmental technology of buildings, theory and structures of buildings, theory and structures of civil engineering works, water resources engineering: October 25th 2023, Bratislava, Slovakia*. Ed. by Andre Bisták. Bratislava: SPEKTRUM STU, 2023, pp. 40–47.
- [26] Jonas Zeifang and Jochen Schütz. “Implicit two-derivative deferred correction time discretization for the discontinuous Galerkin method”. In: *Journal of Computational Physics* (2022), p. 111353.
- [27] Hongkai Zhao. “A fast sweeping method for eikonal equations”. In: *Math. Comput.* (2005).
- [28] D. Zorío, A. Baeza, and P. Mulet. “An Approximate Lax–Wendroff-Type Procedure for High Order Accurate Schemes for Hyperbolic Conservation Laws”. In: *J. Sci. Comput.* (Apr. 2017).

7 Appendix

In this appendix, we formulate nonlinear conditions that the parameters ω and \mathbf{l} in (26) and (27) must satisfy so that the high resolution scheme (17) for the linear advection equation (12) does not produce unphysical oscillations for divergence free velocity. For that purpose, we formulate the conditions when this scheme can be written in the form

$$P_{i,j}(u_{i,j}^{n+1} - u_{i,j}^n) + P_{i+1,j}(u_{i,j}^{n+1} - u_{i+1,j}^{n+1}) + P_{i-1,j}(u_{i,j}^{n+1} - u_{i-1,j}^{n+1}) \\ + P_{i,j+1}(u_{i,j}^{n+1} - u_{i,j+1}^{n+1}) + P_{i,j-1}(u_{i,j}^{n+1} - u_{i,j-1}^{n+1}) = 0, \quad (50)$$

where all five coefficients P are non-negative. Note that these coefficients are different for each discrete equation. Clearly, if (50) is valid, a local discrete minimum and maximum principle [8] is fulfilled as $u_{i,j}^{n+1}$ is a convex combination of all neighboring values. To express (17) in the form (50), all coefficients P must depend on unknown values of the numerical solution.

The first important assumption is that the discrete values of velocities must fulfill the discrete condition of incompressibility $\nabla \cdot \vec{v} = 0$, i.e.,

$$C_{i+1/2,j}^{x,+} + C_{i+1/2,j}^{x,-} - C_{i-1/2,j}^{x,+} - C_{i-1/2,j}^{x,-} + C_{i,j+1/2}^{y,+} + C_{i,j+1/2}^{y,-} - C_{i,j-1/2}^{y,+} - C_{i,j-1/2}^{y,-} = 0. \quad (51)$$

Using (51) multiplied by $u_{i,j}^{n+1}$, one can easily show that the first order scheme (18) of (17) can be transferred to the form (50) with

$$P_{i,j} = 1, \quad P_{i+1,j} = -C_{i+1/2,j}^{x,-}, \quad P_{i-1,j} = C_{i-1/2,j}^{x,+}, \quad P_{i,j+1} = -C_{i,j+1/2}^{y,-}, \quad P_{i,j-1} = C_{i,j-1/2}^{y,+}. \quad (52)$$

Consequently, if the parameters in \mathbf{l} are set to zero in (17), we obtain the first order form of the scheme that produces numerical solutions free of unphysical oscillations.

To subtract (51) multiplied by $u_{i,j}^{n+1}$ from the high resolution scheme (17) with (26) and (27), we express

$$u_{i+1/2,j}^{n+1/2,-} - u_{i,j}^{n+1} = \frac{l_{i,j}^{x,-}}{2} \left(\omega_{i,j}^{x,-} + \frac{1 - \omega_{i,j}^{x,-}}{r_{i,j}^{x,-}} \right) (u_{i,j}^n - u_{i-1,j}^{n+1}) \quad (53)$$

$$u_{i+1/2,j}^{n+1/2,+} - u_{i,j}^{n+1} = - \left(u_{i,j}^{n+1} - u_{i+1,j}^{n+1} - \frac{l_{i+1,j}^{x,+}}{2} (\omega_{i+1,j}^{x,+} r_{i+1,j}^{x,+} + 1 - \omega_{i+1,j}^{x,+}) (u_{i,j}^n - u_{i+1,j}^{n+1}) \right) \quad (54)$$

and analogously for other terms with $u_{i-1/2,j}^{n+1/2,\pm}$ and $u_{i,j\pm 1/2}^{n+1/2,\pm}$. In summary, we obtain the following equations,

$$u_{i,j}^{n+1} - u_{i,j}^n + C_{i+1/2,j}^{x,+} \frac{l_{i,j}^{x,-}}{2} \left(\omega_{i,j}^{x,-} + \frac{1 - \omega_{i,j}^{x,-}}{r_{i,j}^{x,-}} \right) (u_{i,j}^n - u_{i-1,j}^{n+1}) \\ - C_{i+1/2,j}^{x,-} \left(u_{i,j}^{n+1} - u_{i+1,j}^{n+1} - \frac{l_{i+1,j}^{x,+}}{2} (\omega_{i+1,j}^{x,+} r_{i+1,j}^{x,+} + 1 - \omega_{i+1,j}^{x,+}) (u_{i,j}^n - u_{i+1,j}^{n+1}) \right) \\ - C_{i-1/2,j}^{x,-} \frac{l_{i,j}^{x,+}}{2} \left(\omega_{i,j}^{x,+} + \frac{1 - \omega_{i,j}^{x,+}}{r_{i,j}^{x,+}} \right) (u_{i,j}^n - u_{i+1,j}^{n+1}) \\ + C_{i-1/2,j}^{x,+} \left(u_{i,j}^{n+1} - u_{i-1,j}^{n+1} - \frac{l_{i-1,j}^{x,-}}{2} (\omega_{i-1,j}^{x,-} r_{i-1,j}^{x,-} + 1 - \omega_{i-1,j}^{x,-}) (u_{i,j}^n - u_{i-1,j}^{n+1}) \right) + \dots = 0, \quad (55)$$

where we have skipped analogous terms that should appear after $C_{i,j\pm 1/2}^{y,\pm}$. Taking into account that

$$u_{i,j}^n - u_{i\pm 1,j}^{n+1} = u_{i,j}^{n+1} - u_{i\pm 1,j}^{n+1} - (u_{i,j}^{n+1} - u_{i,j}^n),$$

the equations (55) can be written in the form (50) with the coefficients

$$P_{i-1,j} = C_{i+1/2,j}^{x,+} l_{i,j}^{x,-} A_{i,j}^{x,-} + C_{i-1/2,j}^{x,+} (1 - A_{i-1,j}^{x,-}), \quad P_{i+1,j} = -C_{i-1/2,j}^{x,-} l_{i,j}^{x,+} A_{i,j}^{x,+} - C_{i+1/2,j}^{x,-} (1 - A_{i+1,j}^{x,+}) \quad (56)$$

$$P_{i,j-1} = C_{i,j+1/2}^{y,+} l_{i,j}^{y,-} A_{i,j}^{y,-} + C_{i,j-1/2}^{y,+} (1 - A_{i,j-1}^{y,-}), \quad P_{i,j+1} = -C_{i,j-1/2}^{y,-} l_{i,j}^{y,+} A_{i,j}^{y,+} - C_{i,j+1/2}^{y,-} (1 - A_{i,j+1}^{y,+}) \quad (57)$$

$$\begin{aligned} P_{i,j} = & 1 - C_{i+1/2,j}^{x,+} l_{i,j}^{x,-} A_{i,j}^{x,-} + C_{i-1/2,j}^{x,+} A_{i-1,j}^{x,-} + C_{i-1/2,j}^{x,-} l_{i,j}^{x,+} A_{i,j}^{x,+} - C_{i+1/2,j}^{x,-} A_{i+1,j}^{x,+} \\ & - C_{i,j+1/2}^{y,+} l_{i,j}^{y,-} A_{i,j}^{y,-} + C_{i,j-1/2}^{y,+} A_{i,j-1}^{y,-} + C_{i,j-1/2}^{y,-} l_{i,j}^{y,+} A_{i,j}^{y,+} - C_{i,j+1/2}^{y,-} A_{i,j+1}^{y,+}. \end{aligned} \quad (58)$$

where the coefficients A are defined by

$$A_{i,j}^{x,\pm} := \frac{1}{2} \left(\omega_{i,j}^{x,\pm} + \frac{1 - \omega_{i,j}^{x,\pm}}{r_{i,j}^{x,\pm}} \right), \quad A_{i\pm 1,j}^{x,\pm} := \frac{l_{i\pm 1,j}^{x,\pm}}{2} (\omega_{i\pm 1,j}^{x,\pm} r_{i\pm 1,j}^{x,\pm} + 1 - \omega_{i\pm 1,j}^{x,\pm}) \quad (59)$$

and

$$A_{i,j}^{y,\pm} := \frac{1}{2} \left(\omega_{i,j}^{y,\pm} + \frac{1 - \omega_{i,j}^{y,\pm}}{r_{i,j}^{y,\pm}} \right), \quad A_{i,j\pm 1}^{y,\pm} := \frac{l_{i,j\pm 1}^{y,\pm}}{2} (\omega_{i,j\pm 1}^{y,\pm} r_{i,j\pm 1}^{y,\pm} + 1 - \omega_{i,j\pm 1}^{y,\pm}). \quad (60)$$

To prove the sign properties for the coefficients P , we are inspired by limiter techniques that exist in many variants [13, 10]. We follow the simplest and robust approach without an attempt to optimize the definitions of ω and l to maximize accuracy.

Firstly, we require $l_{i,j}^{*,\pm} = 0$ if $r_{i,j}^{*,\pm} < 0$ with $*$ = x and $*$ = y . Note that the ratios in r take negative values only near extrema of numerical solutions. Having this requirement, it is enough to consider only positive values of ratios in r . In such case, to have non-negative coefficients $P_{i\pm 1,j}$ and $P_{i,j\pm 1}$ for any values of parameters in l in the interval $[0, 1]$, it is enough to require

$$A_{i\pm 1,j}^{x,\pm} \leq 1, \quad A_{i,j\pm 1}^{y,\pm} \leq 1. \quad (61)$$

The inequalities (61) are satisfied trivially by the ENO method (33) for positive ratios in r .

Finally, to prove the sign property for $P_{i,j}$, we have to use the parameters $l_{i,j}^{*,\pm}$. Note that for positive ratios in r , the coefficients $A_{i,j}^{*,\pm}$, $A_{i\mp 1,j}^{*,\pm}$, and $A_{i,j\mp 1}^{*,\pm}$ are non-negative. Using the definition of the parameter C in (30), we can estimate

$$\begin{aligned} P_{i,j} \geq & 1 - C l_{i,j}^{x,-} A_{i,j}^{x,-} + C_{i-1/2,j}^{x,+} A_{i-1,j}^{x,-} - C l_{i,j}^{x,+} A_{i,j}^{x,+} - C_{i+1/2,j}^{x,-} A_{i+1,j}^{x,+} \\ & - C l_{i,j}^{y,-} A_{i,j}^{y,-} + C_{i,j-1/2}^{y,+} A_{i,j-1}^{y,-} - C l_{i,j}^{y,+} A_{i,j}^{y,+} - C_{i,j+1/2}^{y,-} A_{i,j+1}^{y,+}, \end{aligned} \quad (62)$$

so to obtain $P_{i,j} \geq 0$ we can require (if $C > 1$)

$$\begin{aligned} & l_{i,j}^{x,-} A_{i,j}^{x,-} + l_{i,j}^{x,+} A_{i,j}^{x,+} + l_{i,j}^{y,-} A_{i,j}^{y,-} + l_{i,j}^{y,+} A_{i,j}^{y,+} \leq \\ & \frac{1}{C} \left(1 + C_{i-1/2,j}^{x,+} A_{i-1,j}^{x,-} - C_{i+1/2,j}^{x,-} A_{i+1,j}^{x,+} + C_{i,j-1/2}^{y,+} A_{i,j-1}^{y,-} - C_{i,j+1/2}^{y,-} A_{i,j+1}^{y,+} \right). \end{aligned} \quad (63)$$

Clearly, there are many ways how to define the parameters l , in theory, to satisfy (63). For any such definition, the high resolution scheme (17) will represent nonlinear system of algebraic equations. In our current approach given by (29), we use iterative methods in the form of predictor-corrector scheme together with dimensional splitting and fast sweeping method. We plan to develop more involved definitions of parameters l in future.